Ultrahigh-resolution spectroscopy with atomic or molecular dark resonances: Exact steady-state line shapes and asymptotic profiles in the adiabatic pulsed regime

Thomas Zanon-Willette*
UPMC Univ. Paris 06, UMR 7092, LPMAA, 4 place Jussieu, case 76, F-75005 Paris, France, and CNRS, UMR 7092, LPMAA, 4 place Jussieu, case 76, F-75005 Paris, France

Emeric de Clercq
LNE-SYRTE, Observatoire de Paris, CNRS, UPMC, 61 avenue de l'Observatoire, F-75014 Paris, France

Ennio Arimondo
Dipartimento di Fisica "E. Fermi," Università di Pisa, Lgo. B. Pontecorvo 3, I-56122 Pisa, Italy
(Received 10 October 2011; published 2 December 2011)

Exact and asymptotic line shape expressions are derived from the semiclassical density matrix representation describing a set of closed three-level Λ atomic or molecular states including decoherences, relaxation rates, and light shifts. An accurate analysis of the exact steady-state dark-resonance profile describing the Autler-Townes doublet, the electromagnetically induced transparency or coherent population trapping resonance, and the Fano-Feshbach line shape leads to the linewidth expression of the two-photon Raman transition and frequency shifts associated to the clock transition. From an adiabatic analysis of the dynamical optical Bloch equations in the weak field limit, a pumping time required to efficiently trap a large number of atoms into a coherent superposition of long-lived states is established. For a highly asymmetrical configuration with different decay channels, a strong two-photon resonance based on a lower states population inversion is established when the driving continuous-wave laser fields are greatly unbalanced. When time separated resonant two-photon pulses are applied in the adiabatic pulsed regime for atomic or molecular clock engineering, where the first pulse is long enough to reach a coherent steady-state preparation and the second pulse is very short to avoid repumping into a new dark state, dark-resonance fringes mixing continuous-wave line shape properties and coherent Ramsey oscillations are created. Those fringes allow interrogation schemes bypassing the power broadening effect. Frequency shifts affecting the central clock fringe computed from asymptotic profiles and related to the Raman decoherence process exhibit nonlinear shapes with the three-level observable used for quantum measurement. We point out that different observables experience different shifts on the lower-state clock transition.

DOI: 10.1103/PhysRevA.84.062502 PACS number(s): 32.70.Jz, 32.80.Qk, 37.10.Jk, 06.20.Jr

I. INTRODUCTION

In the 1930s, molecular-beam magnetic resonance techniques achieved very high precision allowing the observation of atomic and molecular systems essentially in total isolation [1]. The Rabi method revealed coupling interactions between internal energy states and provided plenty of information not only on atomic and molecular structure, but also on nuclear properties. In the 1950s, Ramsey realized a scheme with much higher resolution by increasing the interaction time between the atom or molecule and the oscillating field [2]. Still today, this technique provides the highest resolution in order to follow a dynamical evolution of wave functions and probe their phase accumulations. Control and elimination of systematic frequency shifts dephasing a wave function oscillation at a natural Bohr frequency are fundamental tasks to achieve precision measurement [3].

An alternative tool to probe by the Rabi or Ramsey sequences, for a dipole-forbidden transition, is to radiatively mix the atomic or molecular states. As an example, without natural state mixing from a spin-orbit interaction, a long-lived Raman coherence between a ground state and a long-lived (as in alkali metals) or metastable (as in two-electron atoms) level, to be referred as clock states, can be established by a two-photon process via an upper excited level, thus forming a three-level Λ system. The properties of such a system are strongly determined by an optical pumping mechanism leading to a formation of a dark resonance associated with a trapping of the atomic population in a coherent superposition of states [4–10]. Since such quantum superposition states are radiatively stable, the associated Raman coherence production leads to extremely narrow dark resonances allowing high-resolution frequency measurements [11]. Such coherences were explored for single trapped ions [12,13], microwave clocks [14], microwave chips [15,16], optical lattice clocks [17], multiphoton excitations [18,19], and nuclear clocks [20]. Similar coherent superpositions are used in solid-state physics for quantum information [21], in superconducting circuits [22,23], in a single impurity ion inserted into a crystal [24], in quantum dots [25] with protection against random nuclear spin interactions [26], and in optomechanical systems [27,28]. They are also actively considered within the future challenge of realizing nuclear systems for quantum optics in the x-rays region [29,30]. Dark resonances, largely exploited in quantum optics, have been extended to the preparation of molecules in rovibrational ground states [31] and to coherent superposition of atomic or molecular states in order to measure atomic

*thomas.zanon@upmc.fr

scattering lengths and lifetimes of exotic molecular states [32–35].

Three-level narrow resonances are associated to quantum interferences produced by amplitude scattering into different channels and are strongly dependent on the configuration intensities and detunings [36,37]. Such different line shapes were associated to quantum interferences as the Autler-Townes (AT) splitting of the resonance [38], the Fano-Feshbach (FF) canonical form [39], and the dark-resonance (DR) line shape [8] known as coherent population trapping (CPT) [6,40] or electromagnetically induced transparency (EIT) [41,42].

Accurate calculation of the line shape for a quantum superposition resonance requires numerical integration of the Bloch's equations. The literature reports on efforts to establish approximate analytic equations applicable to each particular case and, in a few cases, exact but rather complex ones [5,10,43–48]. The application of Λ schemes to high accuracy atomic clocks, in microwave or optical domains, requires us to determine precisely the physical processes affecting the resonance line shape and the shifts of the clock frequency. For that purpose this work provides a careful analysis of the line shape dependence on different parameters characterizing the atomic or molecular system under investigation.

The standard clock interrogation of a three-level system involves continuous excitation of the two lower states while sweeping through the Raman resonance. For that regime, starting from the steady-state analytical solution of three-level optical Bloch equations, we derive the exact expression of the resonance line shape where the role of the relaxations and dephasing rates determining the absorption profile is expressed with a physical meaning. Our detailed discussion of key line shape parameters expands previous analysis [5,6,10,13,36,37]. We show that Autler-Townes, CPT, EIT and FF line shapes are associated to a universal two-photon resonance line shape depending on system parameters [49]. The analytical expressions for the frequency shift associated either to the FF extrema or to the EIT resonance point out dependencies not obvious in a perturbation treatment.

An alternative clock operation scheme is based on a Raman-Ramsey scheme with the application of time separated but resonant two-photon pulses, experimentally introduced in the microwave domain [50,51] and extended to rubidium cold atoms [52]. This operation was inspired by the Ezekiel's group work at MIT on a thermal beam of sodium atoms [53]. While in the standard Ramsey approach, a coherent superposition of clock states in the bare atomic or molecular basis is dynamically produced by a $\pi/2$ pulse depending on pulse duration and laser power; the coherent superposition, in the three-level two-photon approach, is created by an optical pumping process long enough to reach a steady state. This scheme overcomes the power broadening mechanism of the continuous-wave resonance allowing us to obtain high contrasted signals in a saturation regime. This idea was extended in Refs. [54–56] to the realization of EIT-Raman (and hyper-Raman) optical clocks with alkaline-earth-metal atoms. The time-separated and individually tailored laser pulses may be designed to create an atomic coherent superposition while eliminating offresonant ac Stark contributions from external levels modifying the optical clock resonance [54]. For the regime of the first laser pulse long enough to produce an efficient coherent superposition, we present here a detailed analysis describing the dependence of the DR line shape on the system parameters.

Within the quantum clock framework, the determination of line shapes and resonance shifts in different experimental configurations remains an important issue, to be carefully investigated within the present work. An important result of the present analytical and numerical analysis for the resonance frequency shift of a three-level quantum clock is that different line shapes versus the optical detunings are obtained depending on the experimentally detected population or coherence observable.

The Λ system and the Bloch's equations for an homogeneous medium are introduced in Sec. II, where an adiabatic analysis of the time dependent equations determines the approximated time scale required to produce an efficient atomic or molecular coherent superposition. Section III establishes an exact treatment of the excited state steady-state regime and derives the key informations on the dark-resonance line shape. In Sec. IV, we derive the steady-state profile of a two-photon resonance between clock states. In Sec. V, we focus our attention on the Raman coherence line shape observed between clock states. Finally Sec. VI analyzes DR fringes produced with resonant two-photon pulses separated in time mixing steady-state properties and Ramsey oscillations. A detailed analysis of the fringe properties is derived in the adiabatic regime where the first pulse establishes a steady-state solution and the probe pulse duration vanishes. Instead only dynamical properties of these phase shifts were demonstrated in Refs. [54,55,57,58]. In the Appendix A, we rewrite line shape population solutions in terms of generalized multiphoton transition rates enhancing one- and two-photon transition rates in the three-level system. We finally derive in Appendix B a first order analytical expression of the central fringe Raman frequency shift associated to the pulsed dark-resonance line shape.

II. THREE-LEVEL OPTICAL BLOCH EQUATIONS

The Doppler-free three-level system presented in Fig. 1 is described by the density matrix ρ_{ij} $(i,j = 1,2,3)$ obeying the Liouville equation

$$\frac{d}{dt}\rho_{ij} = \frac{1}{i\hbar}\sum_k (H_{i,k}\rho_{k,j} - \rho_{i,k}H_{k,j}) + \mathcal{R}\rho_{ij}. \tag{1}$$

The coupling of the three atomic or molecular states to two coherent radiation fields, see Fig. 1, is described within the rotating wave approximation (RWA) by the following Hamiltonian:

$$H = \hbar\begin{pmatrix} \Delta_1 & 0 & \Omega_1 \\ 0 & \Delta_2 & \Omega_2 \\ \Omega_1 & \Omega_2 & 0 \end{pmatrix}, \tag{2}$$

where Δ_1 and Δ_2 are the detunings of the two fields. Depending on the transition the Rabi frequencies Ω_1 and Ω_2 driving the system are determined by the product either between the electric dipole and the electric field amplitude or between the magnetic dipole and the magnetic field amplitude. It is worth noticing that Rabi frequencies defined here are half of the definition of Ref. [59]. The matrix $\mathcal{R}\rho_{ij}$ taking into

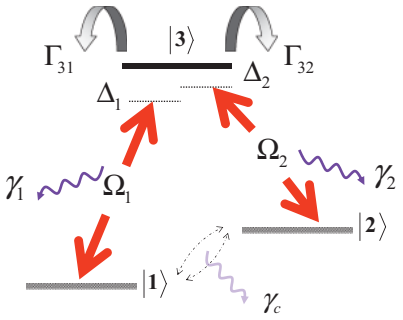

FIG. 1. (Color online) Closed three-level Λ configuration in the density matrix representation including relaxation rates Γ_{31},Γ_{32}, and decoherences $\gamma_1,\gamma_2,\gamma_c$. Optical detunings are Δ_1, Δ_2. The parameter $\delta_r = \Delta_1 - \Delta_2$ defines the Raman resonance condition. Ω_1 and Ω_2 define the couplings with the applied laser fields. $|1\rangle$ and $|2\rangle$ are the clock states while $|3\rangle$ is the excited state.

account relaxation and decoherence phenomena is written

$$\mathcal{R}\rho_{ij} = \begin{pmatrix} \Gamma_{31}\rho_{33} & -\gamma_c\rho_{12} & -\gamma_1\rho_{13} \\ -\gamma_c\rho_{21} & \Gamma_{32}\rho_{33} & -\gamma_2\rho_{23} \\ -\gamma_1\rho_{31} & -\gamma_2\rho_{32} & -\Gamma\rho_{33} \end{pmatrix}. \tag{3}$$

The total spontaneous emission rate Γ is composed by the Γ_{31},Γ_{32} rates (with $\Gamma = \Gamma_{31} + \Gamma_{32}$) describing either an alkaline ($\Gamma_{31} \approx \Gamma_{32}$) or an alkaline-earth ($\Gamma_{31} \neq \Gamma_{32}$) three-level decay configuration. Optical coherences are relaxed with terms γ_1,γ_2, where $\gamma_1 + \gamma_2 = \gamma$. In a pure radiative process [59], optical decoherences are related to spontaneous emission rates by the relation $\gamma_1 = \gamma_2 = (\Gamma_{31} + \Gamma_{32})/2$. The ρ_{12} decoherence is described by the γ_c dephasing term. The optical Bloch equations describe the temporal evolution of the density matrix elements in the RWA as [49]

$$\begin{aligned} \frac{d\rho_{11}}{dt} &= -2\Omega_1 \mathrm{Im}\{\rho_{13}\} + \Gamma_{31}\rho_{33}, \\ \frac{d\rho_{22}}{dt} &= -2\Omega_2 \mathrm{Im}\{\rho_{23}\} + \Gamma_{32}\rho_{33}, \\ \frac{d\rho_{33}}{dt} &= 2\Omega_1 \mathrm{Im}\{\rho_{13}\} + 2\Omega_2 \mathrm{Im}\{\rho_{23}\} - \Gamma\rho_{33}, \\ \frac{d\rho_{13}}{dt} &= -[\gamma_1 + i\Delta_1]\rho_{13} + i\Omega_2\rho_{12} - i\Omega_1(\rho_{33} - \rho_{11}), \\ \frac{d\rho_{23}}{dt} &= -[\gamma_2 + i\Delta_2]\rho_{23} + i\Omega_1\rho_{21} - i\Omega_2(\rho_{33} - \rho_{22}), \\ \frac{d\rho_{12}}{dt} &= -[\gamma_c + i(\Delta_1 - \Delta_2)]\rho_{12} + i\Omega_2\rho_{13} - i\Omega_1\rho_{32}, \end{aligned} \tag{4}$$

with $\rho_{ji} = \rho_{ij}^*$. The population conservation of the closed system is given by $\rho_{11} + \rho_{22} + \rho_{33} = 1$. The optical detunings will be related to the Raman detuning δ_r by $\Delta_1 = \Delta_0$ and $\Delta_2 = \Delta_0 - \delta_r$. Δ_0 represents the common optical detuning for a configuration where one laser is fixed while the other is frequency scanned. Notice that within the approach of deriving the Δ_1,Δ_2 laser modes from a single source by modulation at frequency δ_r, with $\Delta_1 = \Delta_0 \pm \delta_r/2$ and $\Delta_2 = \Delta_0 \mp \delta_r/2$, the light-shift derivation should be modified.

Equations (4) describe the transient dynamics and the steady state of populations and quantum coherences. A complete state mixing is reached when all atoms or molecules have been pumped efficiently into the dark state, a coherent superposition of the lower states. Thus, a pumping time is required to achieve an optimal atomic fraction trapped into the coherent state superposition. We derive such time scale evolution from Eq. (4) by an adiabatic elimination of the time derivative, $d\rho_{33}(t)/dt = d\rho_{13}(t)/dt = d\rho_{23}(t)/dt \equiv 0$ for pulse durations greater than $\Gamma_{31}^{-1},\Gamma_{32}^{-1}$, as the population ρ_{33} and optical coherences ρ_{23} and ρ_{13} evolve more quickly than the populations ρ_{11}, ρ_{22} and the Raman coherence ρ_{12}.

We investigate the dynamics of the three-level Λ systems using various combinations of long and short two-photon pulses separated in time. A straightforward temporal analysis of the resulting adiabatic set, similar to NMR equations [60,61], exhibits two damping times: τ_{osc}, determining the phase memory of the Raman coherence precession (equivalent to a transversal or spin-spin relaxation rate), and τ_p, which determines the typical population transfer into the dark state superposition (similar to a longitudinal or spin-lattice relaxation rate) [62]. At low optical saturation $\Omega_1,\Omega_2 \ll \Gamma,\gamma$, we have

$$\begin{aligned} \tau_{\mathrm{osc}}(\Delta_0) &\sim \left(\gamma_c + \frac{\Omega_1^2}{\widetilde{\gamma}_2} + \frac{\Omega_2^2}{\widetilde{\gamma}_1}\right)^{-1}, \\ \tau_{\mathrm{p}}(\Delta_0) &\sim \left(\frac{\Omega_1^2}{\widetilde{\gamma}_1} + \frac{\Omega_2^2}{\widetilde{\gamma}_2}\right)^{-1}\left[1 + \widetilde{\Upsilon}\frac{\Omega_2^2/\widetilde{\gamma}_2 - \Omega_1^2/\widetilde{\gamma}_1}{\Omega_2^2/\widetilde{\gamma}_2 + \Omega_1^2/\widetilde{\gamma}_1}\right]^{-1}, \end{aligned} \tag{5}$$

where we have introduced the following generalized relaxation rates:

$$\widetilde{\gamma}_i = \frac{\Delta_i^2 + \gamma_i^2}{\gamma_i}, \quad i = 1,2. \tag{6}$$

The $\widetilde{\Upsilon}$ generalized branching ratio difference is

$$\widetilde{\Upsilon} = \frac{\frac{3}{\Gamma}\left(\Omega_1^2/\widetilde{\gamma}_1 - \Omega_2^2/\widetilde{\gamma}_2\right) + \Upsilon}{\frac{3}{\Gamma}\left(\Omega_1^2/\widetilde{\gamma}_1 + \Omega_2^2/\widetilde{\gamma}_2\right) + 1}, \tag{7}$$

with the Υ normalized branching ratio given by $\Upsilon = (\Gamma_{31} - \Gamma_{32})/(\Gamma_{31} + \Gamma_{32})$. The τ_{osc} and τ_{p} time scales play a key role on the population transfer between atomic or molecular states [54]. Indeed, optical coherences are efficiently generated only when the Ω_1 and Ω_2 Rabi frequencies are applied for a time τ exceeding $\Gamma_{31}^{-1},\Gamma_{32}^{-1}$. A short pulse duration having $\Gamma_{31}^{-1},\Gamma_{32}^{-1} < \tau < \tau_p$ will be Fourier limited and will lead to a weak contrast resonance profile, whereas a long pulse with $\tau \gg \tau_p \gg \Gamma_{31}^{-1},\Gamma_{32}^{-1}$ will eliminate all time dependencies in line shape and frequency shifts. This regime is latter examined within the following section.

III. THE STEADY-STATE LINE SHAPE OF ρ_{33}

A. The dark resonance

In examining the steady-state situation with all time derivatives in Eq. (4) set to zero, we find the exact expression for the population of the upper state ρ_{33},

$$\rho_{33} = S^{\Lambda}\frac{(\Delta_1 - \Delta_2)^2 + \gamma_c\gamma_{\mathrm{eff}}}{(\Delta_1 - \Delta_2)[\Delta_1 - \Delta_2 - \Delta_f] + \Gamma_{\mathrm{eff}}^2}, \tag{8}$$

where $\Delta_1 - \Delta_2 = \delta_r$ is the Raman detuning. The expression of Δ_f, the frequency shift affecting the Raman detuning, and Γ_{eff}, the half-width of the two-photon resonance, are reported

in the following subsection. The coherence decay rate is $\gamma_{\text{eff}} = \gamma_c + \gamma^*$ with the γ^* saturation rate of the Raman coherence given by

$$\gamma^* = \frac{\Omega_1^2}{\gamma_2} + \frac{\Omega_2^2}{\gamma_1}. \tag{9}$$

Notice that γ_{eff} coincides with τ_{osc}^{-1} for the $\Delta_1 = \Delta_2 = 0$ resonant laser case.

S^Λ of Eq. (8) represents the signal amplitude. It contains the broad features of the ρ_{33} dependence on the optical detunings Δ_1, Δ_2. The fraction on Eq. (8), whose values lie in the [0, 1] interval, determines the ρ_{33} narrow variation with the Raman detuning $\Delta_1 - \Delta_2$. The three-level signal amplitude S^Λ is given by

$$S^\Lambda = \frac{S}{1 + \left(3 - \frac{\Gamma}{\gamma}\right)S + \frac{\overline{\Omega}_2^2\Delta_1^2 + \overline{\Omega}_1^2\Delta_2^2}{\gamma_1\gamma_2}}, \tag{10}$$

where we introduced the normalized dimensionless Rabi frequencies [63]

$$\begin{aligned} \overline{\Omega}_1^2 &= \Omega_1^2 \frac{\Gamma_{32}\gamma_1}{\Omega_1^2\Gamma_{32}\gamma_2 + \Omega_2^2\Gamma_{31}\gamma_1}, \\ \overline{\Omega}_2^2 &= \Omega_2^2 \frac{\Gamma_{31}\gamma_2}{\Omega_1^2\Gamma_{32}\gamma_2 + \Omega_2^2\Gamma_{31}\gamma_1}. \end{aligned} \tag{11}$$

The saturation parameter S driving the population exchange between energy levels is determined from Einstein's rate equations as

$$S = 2\frac{\Omega_1^2\Omega_2^2}{\left(\Gamma_{32}\gamma_2\Omega_1^2 + \Gamma_{31}\gamma_1\Omega_2^2\right)}. \tag{12}$$

The imaginary parts of optical coherences are related to the excited state line shape expression by the relation:

$$\text{Im}\{\rho_{i3}\} = \frac{\Gamma_{3i}}{2\Omega_i}\rho_{33}\,(i = 1,2). \tag{13}$$

Therefore their line shape is equivalent to that of ρ_{33}.

In Appendix A, we recast all population line shapes in terms of multiphoton transitions rates, pointing out the light-shift contributions to the optical detuning terms. We verified that the numerical results to be presented in the following can be derived also from that solution.

Depending on the detuning and intensity of the lasers or microwaves driving the three-level system, the line shapes associated to Eqs. (8) and (13) present very different features, known as AT spectra, the dark or EIT resonance, and the FF profile, associated to different degrees of interference between two-photon transition amplitudes.

The AT profile appears when one Rabi frequency is much larger than the natural linewidth of the excited state ($\Omega_i \gg \Gamma, i = 1,2$), and in addition $\Omega_1 \ll \Omega_2$, or viceversa. Two split resonances, a doublet structure, appears in the frequency spectrum, as shown in Fig. 2(a).

At Rabi frequencies smaller than the excited state width, we reach the DR or EIT configuration where a narrow two-photon resonance is established from the quantum destructive interferences between the transition probability amplitudes [40,42] as seen in Fig. 2(b). The system is placed in the dark state uncoupled from the driving fields. Note that at exact resonance, $\Delta_1 = \Delta_2 = 0$, $\rho_{33} = 0$ when $\gamma_c = 0$. These regimes are characterized ($\Delta_1 \approx \Delta_2 \lesssim \Gamma$) with $\Omega_1 \approx \Omega_2$ for the dark resonance, and $\Omega_i \gg \Omega_j; \Omega_i, \Omega_j < \Gamma$ for the EIT resonance.

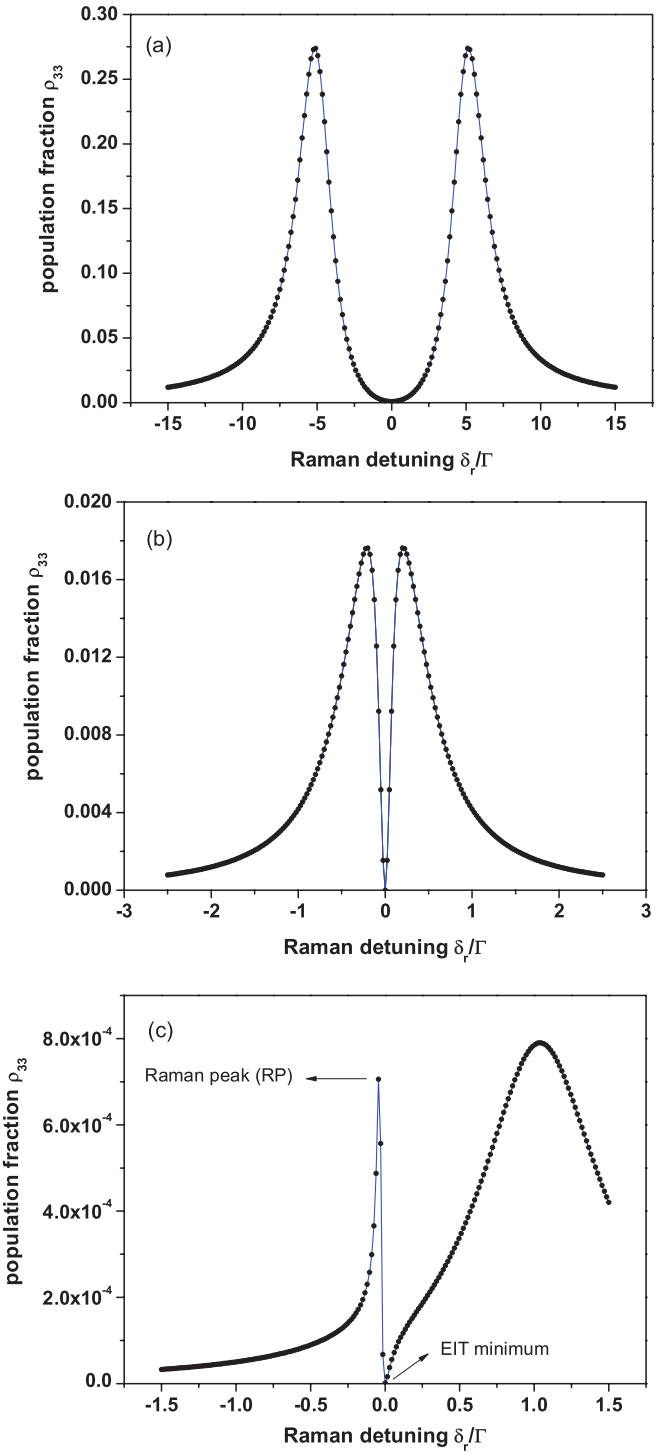

FIG. 2. (Color online) Three-level spectra vs δ_r Raman detuning observed on the ρ_{33} population. For all spectra $\Gamma_{31} = \Gamma_{32} = \Gamma/2$, $\gamma_c = 0$. (a) AT spectrum at $\Delta_0 = 0$, $\Omega_1 = 5\Gamma$, and $\Omega_2 = \Gamma$. (b) Dark-EIT resonance at $\Delta_0 = 0, \Omega_1 = 0.2\Gamma$, and $\Omega_2 = 5 \times 10^{-2}\Gamma$. (c) FF resonance for $\Delta_0 = \Gamma$, $\Omega_1 = 0.2\Gamma$, and $\Omega_2 = 10^{-2}\Gamma$. Solid lines from the analytic solution Eq. (8) and dots from the numerical integration of Eq. (4) at $\tau \gg \tau_p(0)$.

The FF line shape plotted in Fig. 2(c) is originated when one Rabi frequency is much larger than the second one, and in presence of an optical detuning from the excited state($\Omega_i \gg \Omega_j, \Delta_1, \Delta_2 \geqslant \Gamma$). Two resonances appear in the FF spectrum, one broad corresponding to the saturated one-photon resonance. The second sharp feature exhibits a characteristics asymmetric response, highly sensitive to changes in the system parameters and centered around the $\delta_r \approx 0$ Raman detuning. Its minimum is associated to the DR, or EIT dip, while the maximum is the Raman peak, or bright resonance, associated to the preparation of the coherent superposition of $|1\rangle$ and $|2\rangle$ states coupled to the driving electromagnetic fields. Both the EIT dip and the Raman peak are manifestations of the interference between the one-photon and two-photon amplitudes [36]. The asymmetry of the FF profile is reversed by changing the relative ratio between the Rabi frequencies.

B. Γ_{eff} Raman linewidth

The subnatural EIT resonance of Fig. 2(b) experiences a linewidth which is power broadened by the optical saturation rate γ^* of Eq. (9). Let's note that such power broadening is important even for a laser intensity where the saturation is negligible on the optical transitions. In fact Ref. [64] introduced a coherence saturation intensity, defined by $\gamma^* = \gamma_c$, smaller than the optical saturation intensity. The exact expression of the Γ_{eff} Raman half-width is

$$\Gamma_{\text{eff}} = \sqrt{\frac{(\gamma_{\text{eff}} + 3\gamma_c S)\gamma_{\text{eff}}}{1 + \left(3 - \frac{\Gamma}{\gamma}\right)S + \frac{\overline{\Omega}_2^2\Delta_1^2 + \overline{\Omega}_1^2\Delta_2^2}{\gamma_1\gamma_2}}}\sqrt{1+\zeta}, \tag{14}$$

where the factor ζ is

$$\zeta = \frac{\Gamma\frac{\gamma_c S}{2\gamma_1\gamma_2}\left[2\Delta_1\Delta_2 + \Delta_1^2 - \Delta_2^2\right] + \gamma_c^2\frac{\overline{\Omega}_2^2\Delta_1^2 + \overline{\Omega}_1^2\Delta_2^2}{\gamma_1\gamma_2}}{(\gamma_{\text{eff}} + 3\gamma_c S)\gamma_{\text{eff}}} + \frac{\frac{(\gamma_1-\gamma_2)S}{2\gamma_1\gamma_2}(\Gamma_{32}\gamma_2 - \Gamma_{31}\gamma_1)}{\gamma_{\text{eff}} + 3\gamma_c S}. \tag{15}$$

ζ is very small ($\zeta \ll 1$) in a quasiresonant laser interaction (according to the condition $\frac{\gamma_c}{\Gamma}\Delta_1^2, \frac{\gamma_c}{\Gamma}\Delta_2^2 \ll \Omega^2$) and a pure radiative process. As long as $\gamma_c, \Omega_1, \Omega_2 \ll \Gamma$, Γ_{eff} determines the half linewidth of the subnatural resonance. In that regime and for the pure radiative case, Γ_{eff} is well approximated by τ_{osc}^{-1}.

C. Δ_f Raman frequency shift

The frequency shift Δ_f correcting the $\delta_r = 0$ Raman detuning condition is given by

$$\Delta_f = \Delta_{\text{LS}} + \Delta_{\text{DS}}, \tag{16}$$

with the Δ_{LS} light-shift (LS) expression including the saturation effect given by

$$\Delta_{\text{LS}} = \frac{\frac{2}{\gamma_1\gamma_2}\left[\Omega_2^2\overline{\Omega}_2^2\Delta_1 - \Omega_1^2\overline{\Omega}_1^2\Delta_2\right]}{1 + \left(3 - \frac{\Gamma}{\gamma}\right)S + \frac{\overline{\Omega}_2^2\Delta_1^2 + \overline{\Omega}_1^2\Delta_2^2}{\gamma_1\gamma_2}} - \frac{(\gamma_1 - \gamma_2)}{2\gamma_1\gamma_2\gamma}\frac{\Gamma S[\gamma_2\Delta_1 + \gamma_1\Delta_2]}{1 + \left(3 - \frac{\Gamma}{\gamma}\right)S + \frac{\overline{\Omega}_2^2\Delta_1^2 + \overline{\Omega}_1^2\Delta_2^2}{\gamma_1\gamma_2}}. \tag{17}$$

Notice that the second term of the above expression vanishes for the symmetric Λ scheme, i.e., with $\gamma_1 = \gamma_2$ (pure radiative process). In that case, the first term of Δ_{LS} could be associated to the light-shift expression, as pointed out in [5]. The Δ_{DS} decoherence shift (DS) depends on the γ_c rate as

$$\Delta_{\text{DS}} = \gamma_c\frac{S}{2\gamma_1\gamma_2}\frac{[\Gamma(\Delta_1 + \Delta_2) - (\Gamma_{31}\Delta_1 - \Gamma_{32}\Delta_2)]}{1 + \left(3 - \frac{\Gamma}{\gamma}\right)S + \frac{\overline{\Omega}_2^2\Delta_1^2 + \overline{\Omega}_1^2\Delta_2^2}{\gamma_1\gamma_2}}. \tag{18}$$

Let us emphasize that Δ_f is always null at $\Delta_1 = \Delta_2 = 0$ resonance [65].

D. Approximated frequency shifts of EIT and FF resonances

Instead of the previous subsection exact expression correcting the Raman detuning condition in the denominator, it is useful to derive the effective shift of the dark-EIT resonance minimum, which is very relevant for precision spectroscopy or clock resonance. The calculation of the DR/EIT and FF frequency shifts requires us to examine Eq. (8) with the Raman detuning δ_r as a free parameter. A valid approximation for the EIT and Raman-peak shifts in various excitation configurations can be found when optical detuning $\Delta_1 \sim \Delta_2 \sim \Delta_0$ are tuned around the Raman condition $\Delta_1 - \Delta_2 = \delta_r$. A differentiation of Eq. (8) versus the δ_r parameter leads to roots of a quadratic equation defining the following extrema $\delta\omega_{33}(\Delta_0)$ of the EIT/FF line shapes:

$$\delta\omega_{33}(\Delta_0) \approx \frac{\Gamma_{\text{eff}}^2 - \gamma_c\gamma_{\text{eff}}}{\Delta_f}\left(1 \mp \sqrt{1 + \frac{\gamma_c\gamma_{\text{eff}}\Delta_f^2}{\left(\Gamma_{\text{eff}}^2 - \gamma_c\gamma_{\text{eff}}\right)^2}}\right). \tag{19}$$

The $\mp$ solutions refer to the extrema of the FF line shape. The minus (plus) sign holds for EIT dip (Raman Peak) when $\gamma_c\gamma_{\text{eff}}/\Gamma_{\text{eff}}^2 < 1$, and the opposite when $\gamma_c\gamma_{\text{eff}}/\Gamma_{\text{eff}}^2 > 1$. Figure 3 shows the continuous-wave frequency shift versus the common optical detuning Δ_0 using Eq. (19). Results for both $\gamma_c = 5.10^{-4}\Gamma$ and $\gamma_c = 0$ are presented. The EIT decoherence shift, proportional to γ_c, exhibits a linear dependence on the optical detuning when radiative decay terms are symmetrical. As pointed in [10], when the decoherence term vanishes ($\gamma_c = 0$), there is no shift of the EIT minimum [66] except if we take into account external small offresonant level contributions [67]. The Raman peak shift produced by light and decoherence varies with the inverse of the optical detuning as discussed by [37] and observed experimentally in [12]. For a quasiresonant interaction, we can further simplify the above expression for the Raman Peak and the EIT dip when $\gamma_c\gamma_{\text{eff}}/\Gamma_{\text{eff}}^2 \ll 1$ and $\Delta_f^2/\Gamma_{\text{eff}}^2 \ll 1$. Near the two-photon resonance, the shifts of Eq. (19) can be accurately approximated as

$$\delta\omega_{33}^{\text{EIT}}(\Delta_0) \approx -\gamma_c\Delta_f\frac{\gamma_{\text{eff}}}{2\Gamma_{\text{eff}}^2}, \quad \delta\omega_{33}^{RP}(\Delta_0) \approx 2\frac{\Gamma_{\text{eff}}^2}{\Delta_f}. \tag{20}$$

The EIT dip frequency shift is thus roughly given by the product of the γ_c decoherence rate and the Δ_f Raman frequency shift divided by the Γ_{eff} linewidth of the subnatural resonance. Such a dependence was pointed out by [17] and by [46] based on a theoretical analysis of [68], and as mentioned in [48], was earlier derived in [69].

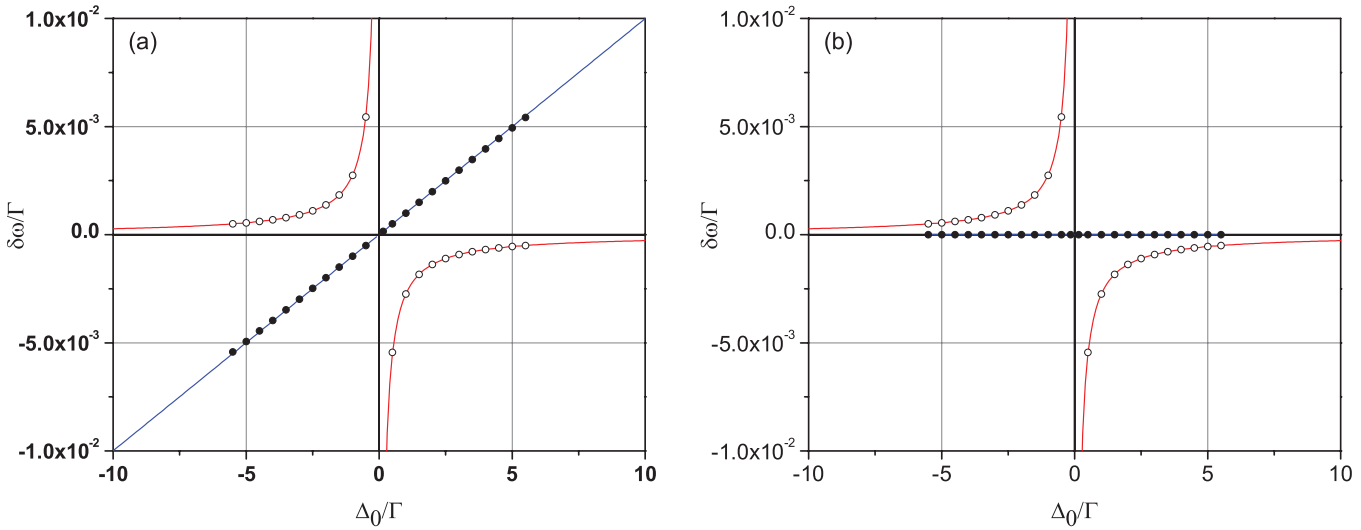

FIG. 3. (Color online) Frequency shifts of the dark-EIT dip and the Raman peak observed on the ρ_{33} excited state population vs the optical detuning Δ_0 from Eq. (19) (straight solid blue line and red lines, respectively) and from the numerical integration of Eq. (4) (solid dots • and open dots ○, respectively). Parameters are $\Gamma_{31} = \Gamma_{32} = \Gamma/2$, $\Omega_1 = 5 \times 10^{-2}\Gamma$, and $\Omega_2 = 10^{-3}\Gamma$. In (a) $\gamma_c = 5 \times 10^{-4}\Gamma$; in (b) $\gamma_c = 0$ leads to a vanishing shift for the EIT resonance.

IV. STEADY-STATE LINE SHAPES OF CLOCK-STATE POPULATIONS ρ_{11}, ρ_{22}

A. The two-photon resonance

We focus now on clock-state resonances observed on the ρ_{11}, ρ_{22} populations and linked to the Raman coherence between those states. The clock-state populations may be expressed in an exact form similar to that of Eq. (8) as

$$\rho_{11} = S^{11}\frac{(\Delta_1-\Delta_2)[\Delta_1-\Delta_2-\Delta_{11}]+\gamma_{11}^2}{(\Delta_1-\Delta_2)[\Delta_1-\Delta_2-\Delta_f]+\Gamma_{\rm eff}^2},$$
$$\rho_{22} = S^{22}\frac{(\Delta_1-\Delta_2)[\Delta_1-\Delta_2+\Delta_{22}]+\gamma_{22}^2}{(\Delta_1-\Delta_2)[\Delta_1-\Delta_2-\Delta_f]+\Gamma_{\rm eff}^2}, \quad (21)$$

where

$$S^{ii} = \left(1+\frac{\widetilde{\gamma}_i\Gamma_{3i}}{2\Omega_i^2}\right)S^{\Lambda}, \quad (i=1,2),$$
$$\Delta_{11} = \overline{\gamma}_{11}(\Delta_1+\gamma_1\overline{\Delta}), \quad \Delta_{22} = \overline{\gamma}_{22}(\Delta_2-\gamma_2\overline{\Delta}), \quad (22)$$
$$\overline{\Delta} = \frac{\Omega_2^2\Gamma_{31}\gamma_2\Delta_1-\Omega_1^2\Gamma_{32}\gamma_1\Delta_2}{\gamma_1\gamma_2(\Omega_2^2\Gamma_{31}+\Omega_1^2\Gamma_{32})},$$

and

$$\gamma_{11}^2 = \gamma_c\gamma_{\rm eff}+\overline{\gamma}_{11}(\gamma_1\gamma_{\rm eff}-\gamma_c\Delta_1\overline{\Delta}),$$
$$\gamma_{22}^2 = \gamma_c\gamma_{\rm eff}+\overline{\gamma}_{22}(\gamma_2\gamma_{\rm eff}+\gamma_c\Delta_2\overline{\Delta}), \quad (23)$$

with

$$\overline{\gamma}_{11} = \frac{\Gamma_{31}\Omega_2^2+\Gamma_{32}\Omega_1^2}{2\Omega_1^2\gamma_1+(\Delta_1^2+\gamma_1^2)\Gamma_{31}},$$
$$\overline{\gamma}_{22} = \frac{\Gamma_{31}\Omega_2^2+\Gamma_{32}\Omega_1^2}{2\Omega_2^2\gamma_2+(\Delta_2^2+\gamma_2^2)\Gamma_{32}}. \quad (24)$$

Figure 4 reports the population resonance under various saturation conditions, matching the AT, EIT, and FF line shapes of Fig. 2. Notice that the EIT regime of Fig. 4(b) corresponds to the case of Rabi frequencies smaller than the natural decay rate of the excited state. The "Lamb-dip"-like line shape for the resulting quasisaturated transition can conveniently be observed in the three-level configuration. This method of spectroscopy without Doppler broadening was proposed and experimentally accomplished by Javan and Schlossberg in [70,71]. In such a situation, the dip can be narrower than the homogeneous linewidth of the population resonance as in Fig. 4(b).

The clock-state populations depend strongly on the normalized branching ratio difference Υ and on the Rabi frequencies driving atomic or molecular transitions. A numerical analysis of [72] demonstrated the occurrence of a strong population transfer for unequal Γ_{31},Γ_{32} decay rates. Figure 5 shows the steady-state complete population transfer for $\Omega_1 \gg \Omega_2$ and $\Upsilon \approx 1$ using the asymmetric decay rates associated to an alkaline-earth three-level system as strontium atoms [17,54]. A large coherent population transfer $\rho_{22} - \rho_{11} = \pm 1$ is achieved when $\Omega_1 \gg \Omega_2$ for $\Upsilon \sim +1$ or $\Omega_2 \gg \Omega_1$ for $\Upsilon \sim -1$.

B. Approximated frequency shift of the two-photon resonance

In an alkaline-earth frequency clock probing scheme, the large population transfer regime of Fig. 5 may be used to detect one lower state population, or the population difference between clock states. Thus, it is important to derive the two-photon shift also in this scheme. Using an analysis equivalent to the derivation of Eq. (19) when $\Delta_1 \sim \Delta_2 \sim \Delta_0$, we obtain the frequency shift of ρ_{11}. For ρ_{22}, we make a similar derivation also using the population conservation condition. We obtain the following expression for $\delta\omega_{11}(\Delta_0)$ and similarly

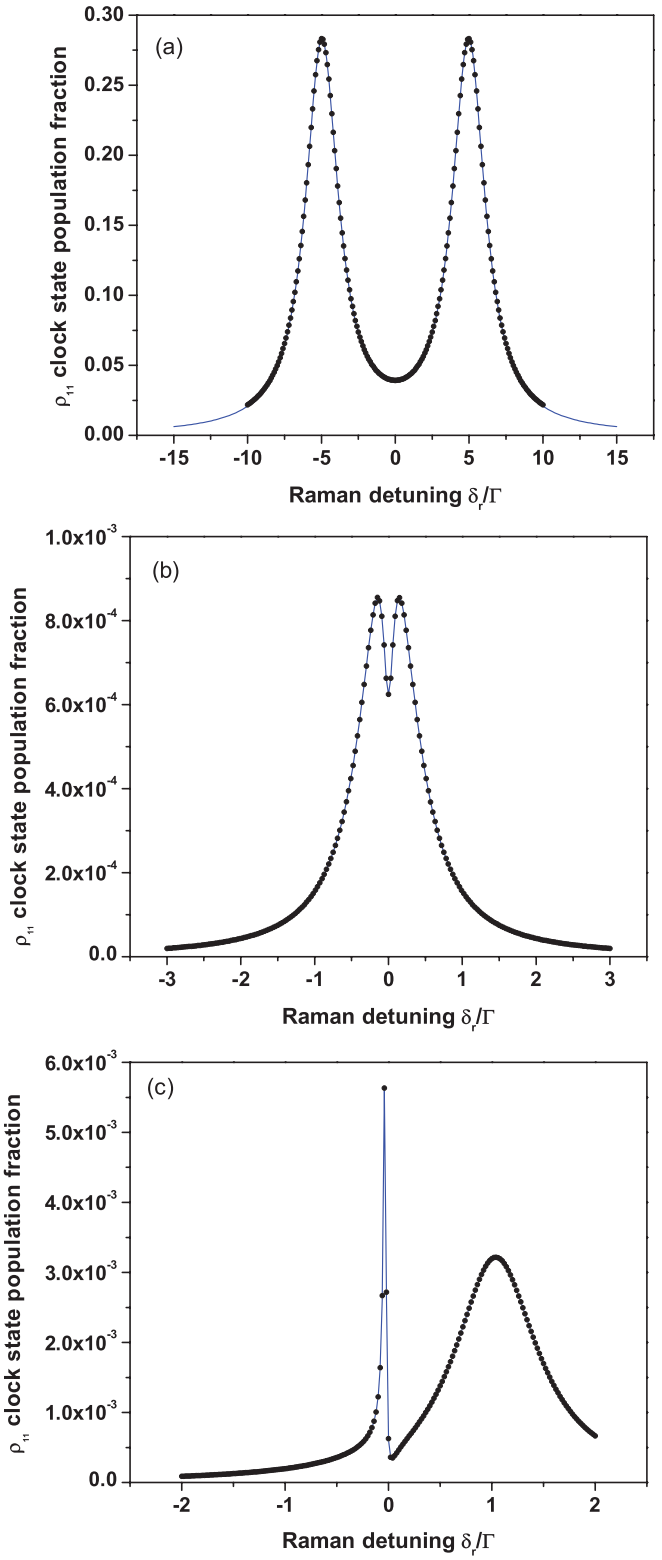

FIG. 4. (Color online) Three-level spectra vs the δ_r Raman detuning observed on the ρ_{11} population using Eq. (21), solid blue line, and the numerical integration of Eq. (4), solid dots (•). In (a) AT resonance, in (b) Lamb-dip line shape, and in (c) FF resonance. System parameters as in Fig. 2. In (a) and (b), Rabi frequencies as in Fig. 2. In (c) $\Omega_1 = 0.2\Gamma$, $\Omega_2 = 5 \times 10^{-3}\Gamma$, and $\Delta_0 = \Gamma$.

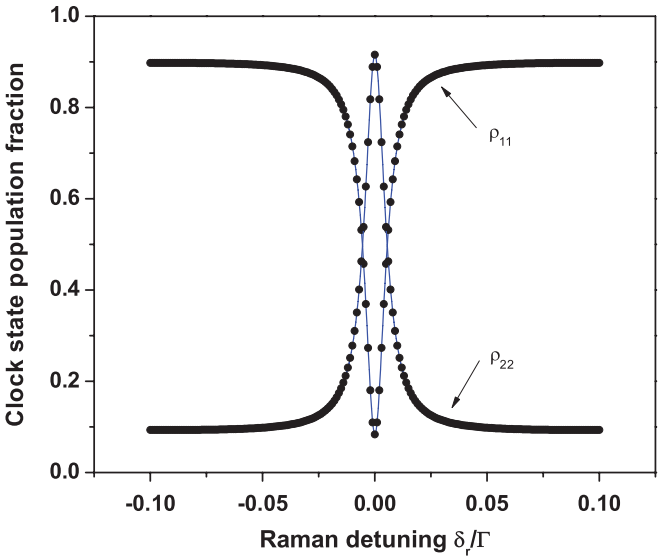

FIG. 5. (Color online) Population inversion resonance between the $|1\rangle$ and $|2\rangle$ states, monitored on ρ_{11} and ρ_{22}, for unbalanced decay rates, $\Gamma_{32} = 10^{-5}\Gamma$, $\Gamma_{31} = \Gamma - \Gamma_{32}$. Solid blue line is computed from Eq. (21), solid dots (•) are the result of the numerical integration of Eq. (4). Other parameters are $\Delta_0 = 0$, $\gamma_c = 0$, $\Omega_1 = 5 \times 10^{-2}\Gamma$, and $\Omega_2 = 5 \times 10^{-4}\Gamma$.

for $\delta\omega_{22}(\Delta_0)$:

$$\delta\omega_{11}(\Delta_0) \sim \delta\omega_{22}(\Delta_0) \approx \frac{\gamma_{11}^2 - \Gamma_{\rm eff}^2}{\Delta_{11} - \Delta_f} \times \left(1 \mp \sqrt{1 + \frac{(\Delta_f - \Delta_{11})\left(\gamma_{11}^2 \Delta_f - \Delta_{11}\Gamma_{\rm eff}^2\right)}{\left(\Gamma_{\rm eff}^2 - \gamma_{11}^2\right)^2}}\right). \tag{25}$$

For the specific radiative configuration of alkaline-earth species shown in Fig. 5, only the solution with the minus sign is needed, but $\mp$ solutions generally refer to the extrema of a dispersive line shape. Our standard choice of the laser detunings $\Delta_1 = \Delta_0$ and $\Delta_2 = \Delta_0 - \delta_r$ introduces a very small difference in expressions of the frequency shifts affecting each clock-state population. For a quasiresonant interaction when $\gamma_c\gamma_{\rm eff}/\Gamma_{\rm eff}^2 \ll 1$ with $\Delta_f/\Gamma_{\rm eff} \ll 1$ and $\Delta_{11}/\Gamma_{\rm eff} \ll 1$, the expression may be simplified to yield

$$\delta\omega_{11}(\Delta_0) \sim \delta\omega_{22}(\Delta_0) \approx \frac{\Delta_{11} - \frac{\gamma_{11}^2}{\Gamma_{\rm eff}^2}\Delta_f}{2\left(1 - \frac{\gamma_{11}^2}{\Gamma_{\rm eff}^2}\right)}. \tag{26}$$

The frequency shift versus the common mode optical detuning Δ_0 affecting the ρ_{11}(equivalently ρ_{22}) resonance is plotted in Figs. 6(a) and 6(b) for two particular ratios of the relaxation rates by spontaneous emission. In both cases, the shift of the two-photon resonance measured on the ρ_{11} or ρ_{22} observables has a dispersive line shape versus the optical detuning Δ_0. The slope is completely reversed owing to a nonlinear behavior when the ratio $\Upsilon \mapsto 1$ as in Fig. 6(b). A comparison with the frequency shift of the excited state ρ_{33} is also included in the figure. Notice the difference in the ρ_{11}/ρ_{33} shifts for the case of a large asymmetry in the spontaneous decay rates.

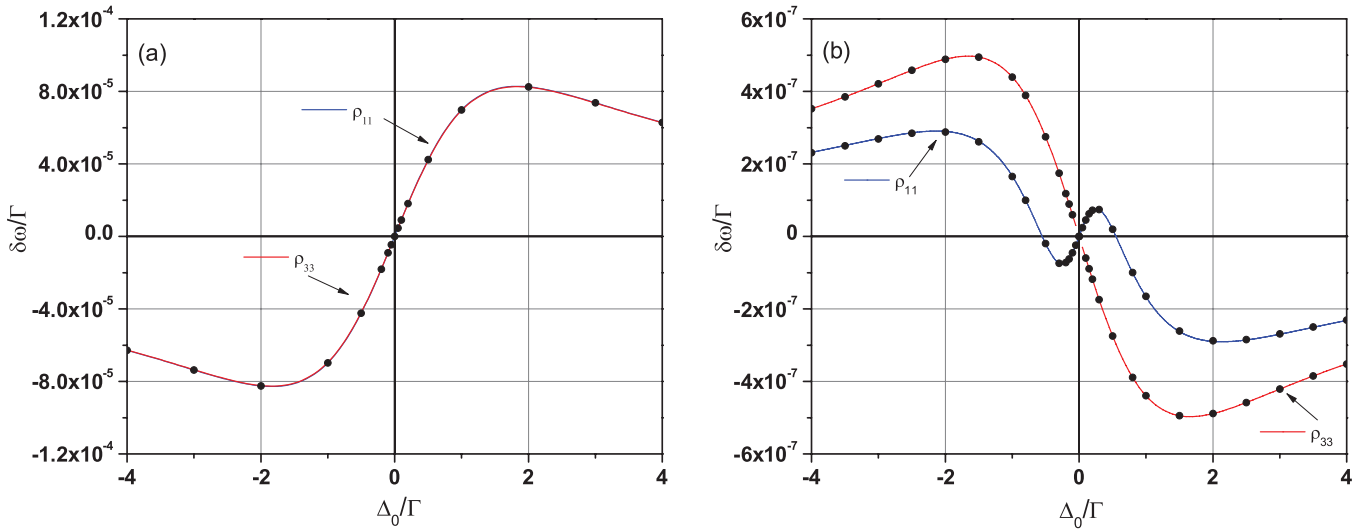

FIG. 6. (Color online) Frequency shift of the population inversion resonance observed on ρ_{11} (or ρ_{22}) as derived from Eq. (25) (solid blue line) and frequency shift of the ρ_{33} EIT resonance from Eq. (19) (solid red line) vs the optical detuning Δ_0, for unbalanced decay rates. Solid dots (•) are from the numerical integration of Eq. (4) with parameters $\Omega_1 = 5\times10^{-2}\Gamma$, $\gamma_c = 510^{-4}\Gamma$, and $\Omega_2 = 5\times10^{-4}\Gamma$. In (a) $\Gamma_{32} = 10^{-5}\Gamma$ and $\Gamma_{31} = \Gamma - \Gamma_{32}$. Note that the $\delta\omega_{33}$ shift is indistinguishable from the $\delta\omega_{11}$ shift. In (b) $\Gamma_{32} = 10^{-10}\Gamma$ and $\Gamma_{31} = \Gamma - \Gamma_{32}$.

V. STEADY-STATE LINE SHAPE OF RAMAN COHERENCE ρ_{12}

A. The Raman coherence resonance

We are now focusing on the steady state Raman coherence resonance $\rho_{12} = \mathrm{Re}\{\rho_{12}\} + i\,\mathrm{Im}\{\rho_{12}\}$ given by

$$\mathrm{Re}\{\rho_{12}\} = \Gamma_{12}S^{\Lambda}\frac{(\Delta_1-\Delta_2)\overline{\Delta}-\gamma_{\mathrm{eff}}}{(\Delta_1-\Delta_2)[\Delta_1-\Delta_2-\Delta_f]+\Gamma_{\mathrm{eff}}^2},$$
$$\mathrm{Im}\{\rho_{12}\} = \Gamma_{12}S^{\Lambda}\frac{(\Delta_1-\Delta_2)+\overline{\Delta}\gamma_c}{(\Delta_1-\Delta_2)[\Delta_1-\Delta_2-\Delta_f]+\Gamma_{\mathrm{eff}}^2}, \tag{27}$$

with

$$\Gamma_{12} = \frac{\Omega_2^2\Gamma_{31}+\Omega_1^2\Gamma_{32}}{2\Omega_1\Omega_2}. \tag{28}$$

When the dipole transition is allowed, the Raman coherence resonance can be detected in several manners. If we deal with alkaline atoms, such as Cs or Rb, the hyperfine Raman coherence might be detected as a microwave emission proportional to $|\rho_{12}|^2$, inserting the atomic medium into a microwave cavity [73]. Figure 7 shows $|\rho_{12}|^2$ versus the Raman detuning condition δ_r when $\Gamma_{31} = \Gamma_{32} = \Gamma/2$ at different values of Δ_0. The dispersive behavior of $\mathrm{Re}\{\rho_{12}\}$ leads to a second resonant peak, appearing when $\Delta_0 > 3\Gamma$ as seen in Figs. 7(b) and 7(c).

B. Approximated frequency shifts of the Raman coherence resonance

We derive here an accurate expression for the frequency-shifted resonance of $|\rho_{12}|^2$ when $\Delta_1 \sim \Delta_2 \sim \Delta_0$. A cubic equation is derived from the analytical differentiation of $|\rho_{12}|^2$ of Eq. (27) with respect to the Raman detuning δ_r. Using Cardan's solutions, the three roots are written as

$$\delta\omega_{12}(\Delta_0) \sim -\frac{b}{3a} + \sqrt{-\frac{p}{3}}\cos\left[\frac{1}{3}\cos^{-1}\left(-\frac{3q}{p}\sqrt{-\frac{3}{p^3}}\right) + 2k\frac{\pi}{3}\right], \tag{29}$$

with $k = 0,1,2$, the p ($p < 0$) and q given by

$$p = \frac{3ac-b^2}{3a^2}, \quad q = \frac{2b^3-9abc+27a^2d}{27a^3}, \tag{30}$$

and

$$\begin{aligned} a &= -1-\overline{\Delta}^2,\\ b &= 3\overline{\Delta}(\gamma_{\mathrm{eff}}-\gamma_c),\\ c &= -2\left(\gamma_c^2\overline{\Delta}^2+\gamma_{\mathrm{eff}}^2\right)+\Gamma_{\mathrm{eff}}^2(1+\overline{\Delta}^2)\\ &\quad +\Delta_f\overline{\Delta}(\gamma_c+\gamma_{\mathrm{eff}}),\\ d &= \Gamma_{\mathrm{eff}}^2\overline{\Delta}(\gamma_c+\gamma_{\mathrm{eff}})+\Delta_f\left(\gamma_c^2\overline{\Delta}^2+\gamma_{\mathrm{eff}}^2\right). \end{aligned} \tag{31}$$

Equation (29) allows us to obtain the frequency shift as a function of the common mode optical detuning Δ_0 plotted in Fig. 8. However an estimate of that shift is obtained looking only at the real part of the coherence solution which mainly describes the line shape emission. From the square modulus of the real part $|\mathrm{Re}\{\rho_{12}\}|^2$, simple cubic solutions for the Raman coherence frequency shift can be derived as

$$\delta\omega_{12}(\Delta_0) \sim \frac{\gamma_{\mathrm{eff}}}{\overline{\Delta}}\left[1 \mp \sqrt{1+\frac{\overline{\Delta}\Gamma_{\mathrm{eff}}}{\gamma_{\mathrm{eff}}}\left(\frac{\overline{\Delta}\Gamma_{\mathrm{eff}}}{\gamma_{\mathrm{eff}}}-\frac{\Delta_f}{\Gamma_{\mathrm{eff}}}\right)}\right], \tag{32}$$

or

$$\delta\omega_{12}(\Delta_0) \sim \frac{\gamma_{\mathrm{eff}}}{\overline{\Delta}}. \tag{33}$$

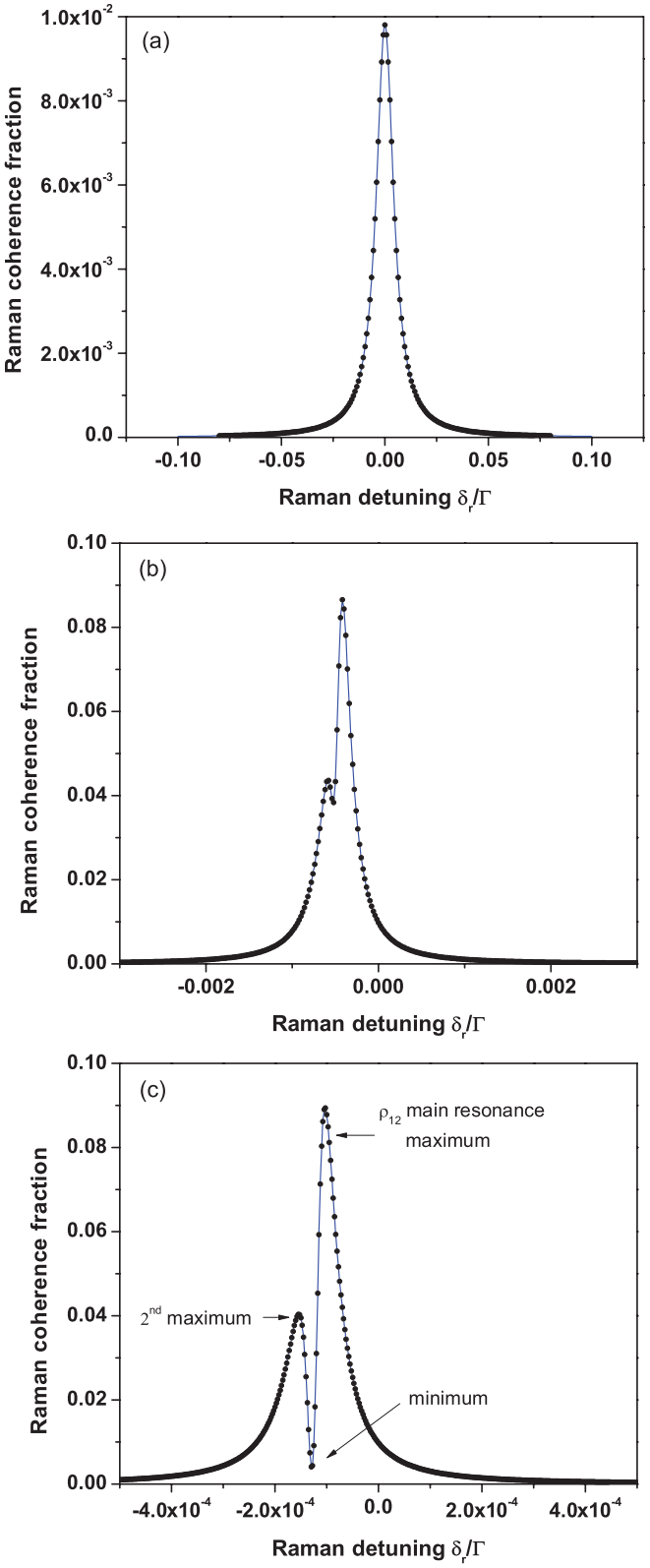

FIG. 7. (Color online) (a) Steady-state line shapes of the $|\rho_{12}|^2$ square modulus vs δ_r using Eq. (27) (solid blue line) for $\Gamma_{31} = \Gamma_{32} = \Gamma/2$, $\Omega_1 = 5 \times 10^{-2}\Gamma$, $\Omega_2 = 5 \times 10^{-3}\Gamma$, and $\gamma_c = 0$. In (a) $\Delta_0 = 0$, in (b) $\Delta_0 = 5\Gamma$, and in (c) $\Delta_0 = 20\Gamma$. Solid dots (•) are from the numerical integration of Eq. (4).

When $\overline{\Delta}\Gamma_{\rm eff}/\gamma_{\rm eff} \ll 1$ and $\Delta_f/\Gamma_{\rm eff} \ll 1$, the Raman coherence frequency-shift expression corresponding to the maximum emission becomes

$$\delta\omega_{12}(\Delta_0) \sim \frac{\Delta_f}{2}. \tag{34}$$

For that case, we recover the usual dispersive shape related to the light-shift $\Delta_{\rm LS}$ affecting clock states. The frequency shift versus the common mode optical detuning Δ_0 derived from Eq. (29) is shown in Fig. 8(a) for the case of a symmetric radiative configuration with $\Gamma_{31} = \Gamma_{32}$ while in Fig. 8(b) for $\Gamma_{31} \gg \Gamma_{32}$. The central dispersive feature, related to the Raman shift expression Δ_f, corresponds to the maximum of the coherent emission. Other branches of the shift correspond to the extrema of the second resonance appearing for $\Delta_0 > 3\Gamma$ as from the line shape simulation of Fig. 7(b). A direct comparison of Fig. 8(b) with frequency shifts reported in Fig. 6 with similar conditions yield to Raman coherence shifts larger by more than an order of magnitude than population frequency shifts.

VI. DARK-RESONANCE FRINGES

A. Pulsed regime line shape

The clock operation may be based on a pulsed Raman-Ramsey scheme, illustrated in Fig. 9, with beating oscillations observed whichever variable is monitored. This detection approach, originally introduced in [53], was refined in [50,51] and discussed in Refs. [54–56]. It allows us to reach a higher precision in the clock frequency measurement, as typical of the Ramsey fringes. The present work focuses on the laser pulse scheme where the first pulse is long enough to allow the atomic or molecular preparation into the dark state superposition and the second delayed short pulse probing that superposition. Because the τ_p pumping time of Eq. (5) is required to reach the steady-state atomic or molecular preparation into the dark state, the length of the first pulse should satisfy $\tau \gg \tau_p(\Delta_0) \gg \Gamma_{31}^{-1}, \Gamma_{32}^{-1}$. From a mathematical point of view, the $\tau \mapsto \infty$ steady state solution of the three-level optical Bloch equations may thus be used as initial condition for determining the evolution at later times. At time τ the laser fields are switched off in order to allow for a free evolution over the time T. Finally a readout operation is performed by applying a short pulse whose time duration τ_m is limited by $\Gamma_{31}^{-1}, \Gamma_{32}^{-1} < \tau_m \ll \tau_p(\Delta_0)$. In this adiabatic regime where $d\rho_{33}(t)/dt = d\rho_{13}(t)/dt = d\rho_{23}(t)/dt \equiv 0$, the short probe pulse operation is well described using the $\tau_m \mapsto 0$ limit. For a readout pulse as long as the preparation pulse, all atoms or molecules are repumped into a new dark state erasing interference fringes. Interferences fringes are detectable on all observables as a function of the T time delay, with very short readout pulses required for optical coherences and the excited state population fraction. Instead longer probing times are required for monitoring fringes on lower state populations due to slow time evolution of the clock states and the Raman coherence.

An analytical expression of the population fraction in the excited state can be established from Eq. (4) in the asymptotic limit of a long preparation pulse and a vanishing read out pulse, i.e., at the end of the free evolution time. In this regime, a pulsed

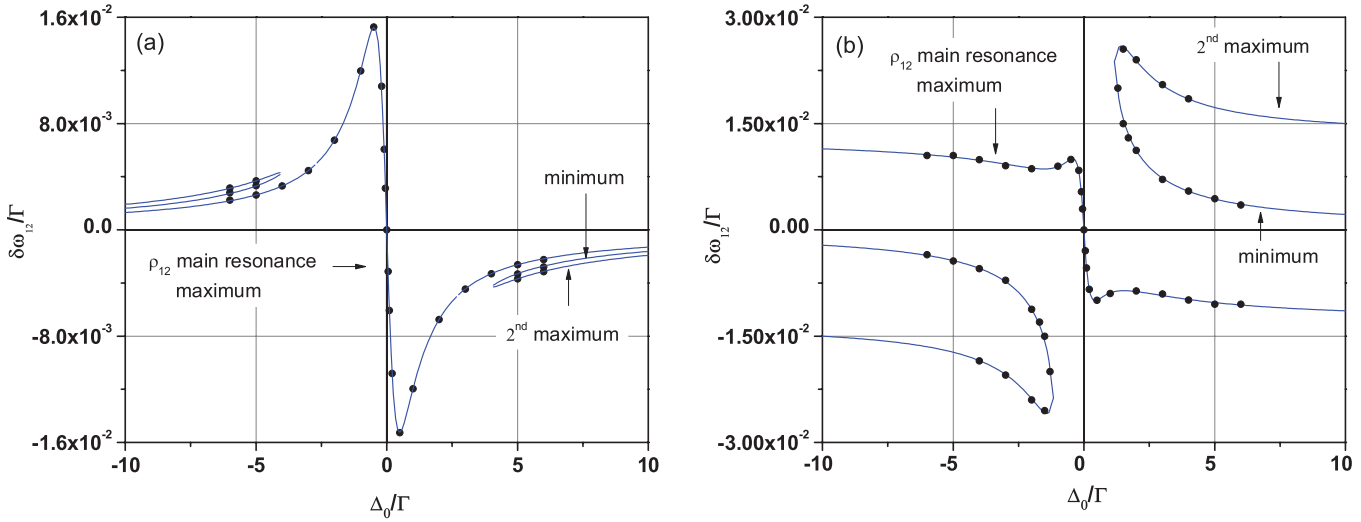

FIG. 8. (Color online) (a) Frequency shift of the Raman coherence resonances observed on the $|\rho_{12}|^2$ as derived from Eq. (29) (solid blue line) vs the optical detuning Δ_0. In (a) we have a symmetric radiative configuration with $\Gamma_{31} = \Gamma_{32} = \Gamma/2$, where $\Omega_1 = 5 \times 10^{-2}\Gamma$, $\Omega_2 = 5 \times 10^{-3}\Gamma$, and $\gamma_c = 0$. In (b) we have an asymmetric radiative configuration with $\Gamma_{31} = \Gamma - \Gamma_{32}$ and $\Gamma_{32} = 10^{-5}\Gamma$, where $\Omega_1 = 5 \times 10^{-2}\Gamma$, $\Omega_2 = 5 \times 10^{-4}\Gamma$, and $\gamma_c = 510^{-4}\Gamma$. Solid dots (•) are from the numerical integration of Eq. (4).

DR expression $\rho_{33}(T)$ and related transmission parts of the $\mathrm{Im}\{\rho_{13}\}(T)$,$\mathrm{Im}\{\rho_{23}\}(T)$ optical coherences can be rewritten in the exact $\alpha_{ij}[1 + \beta_{ij}|\rho_{12}|e^{-\gamma_c T}\cos(\delta_r T - \Phi_{ij})]$ form:

$$\begin{aligned}
\rho_{33}(T) &= \alpha_{33}[1 + \beta_{33}|\rho_{12}|e^{-\gamma_c T}\cos(\delta_r T - \Phi_{33})],\\
\alpha_{33} &= \frac{\Omega_2^2(\Delta n + 1)/\Gamma\widetilde{\gamma}_2 - \Omega_1^2(\Delta n - 1)/\Gamma\widetilde{\gamma}_1}{1 + \frac{3}{\Gamma}\left(\Omega_1^2/\widetilde{\gamma}_1 + \Omega_2^2/\widetilde{\gamma}_2\right)},\\
\beta_{33} &= \frac{\sqrt{\mu_{\gamma 33}^2 + \mu_{\Delta 33}^2}}{\alpha_{33}},\\
\mathrm{Im}\{\rho_{13}\}(T) &= \alpha_{13}[1 + \beta_{13}|\rho_{12}|e^{-\gamma_c T}\cos(\delta_r T - \Phi_{13})],\\
\alpha_{13} &= \frac{\Omega_1}{2\widetilde{\gamma}_1}[3\alpha_{33} + (\Delta n - 1)],
\end{aligned} \tag{35}$$

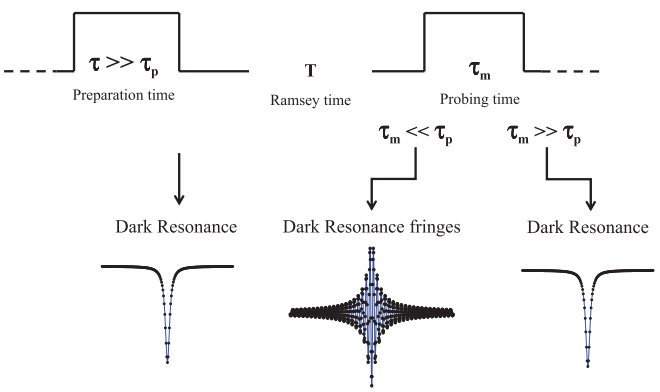

FIG. 9. (Color online) Pulsed dark-resonance detection scheme to perform high-resolution spectroscopy of three-level Λ systems. T is the Ramsey time when both laser light fields Ω_1,Ω_2 are switched off. The first pulse is long enough, $\tau \gg \tau_p(\Delta_0)$, to reach the stationary regime. During the second pulse, the probing time can be short, $\tau_m \ll \tau_p(\Delta_0)$, to observe dark-resonance fringes or long, $\tau_m \gg \tau_p(\Delta_0)$, to recover a cw dark resonance as a new preparation stage for the next pulse.

$$\begin{aligned}
\beta_{13} &= \frac{\sqrt{\mu_{\gamma 13}^2 + \mu_{\Delta 13}^2}}{\alpha_{13}},
\end{aligned} \tag{36}$$

$$\begin{aligned}
\mathrm{Im}\{\rho_{23}\}(T) &= \alpha_{23}[1 + \beta_{23}|\rho_{12}|e^{-\gamma_c T}\cos(\delta_r T - \Phi_{23})],\\
\alpha_{23} &= \frac{\Omega_2}{2\widetilde{\gamma}_2}[3\alpha_{33} - (\Delta n + 1)],\\
\beta_{23} &= \frac{\sqrt{\mu_{\gamma 23}^2 + \mu_{\Delta 23}^2}}{\alpha_{23}}.
\end{aligned} \tag{37}$$

where $\Delta n = \rho_{22} - \rho_{11}$ is the steady-state clock-state population difference obtained from Eq. (21) and $|\rho_{12}|$ is given by Eq. (27). The following quantities were introduced in the above expressions:

$$\begin{aligned}
\mu_{\gamma 33} &= \frac{2\Omega_1\Omega_2}{\Gamma}\left(\frac{(\widetilde{\gamma}_1 + \widetilde{\gamma}_2)/\widetilde{\gamma}_1\widetilde{\gamma}_2}{1 + \frac{3}{\Gamma}\left(\Omega_1^2/\widetilde{\gamma}_1 + \Omega_2^2/\widetilde{\gamma}_2\right)}\right),\\
\mu_{\Delta 33} &= \frac{2\Omega_1\Omega_2}{\Gamma}\left(\frac{\Delta_1/\widetilde{\gamma}_1\gamma_1 - \Delta_2/\widetilde{\gamma}_2\gamma_2}{1 + \frac{3}{\Gamma}\left(\Omega_1^2/\widetilde{\gamma}_1 + \Omega_2^2/\widetilde{\gamma}_2\right)}\right),
\end{aligned} \tag{38}$$

$$\begin{aligned}
\mu_{\gamma 13} &= \frac{3}{2}\frac{\Omega_1}{\widetilde{\gamma}_1}\mu_{\gamma 33} - \frac{\Omega_2}{\widetilde{\gamma}_1},\\
\mu_{\Delta 13} &= \frac{3}{2}\frac{\Omega_1}{\widetilde{\gamma}_1}\mu_{\Delta 33} - \Omega_2\frac{\Delta_1}{\gamma_1\widetilde{\gamma}_1},
\end{aligned} \tag{39}$$

$$\begin{aligned}
\mu_{\gamma 23} &= \frac{3}{2}\frac{\Omega_2}{\widetilde{\gamma}_2}\mu_{\gamma 33} - \frac{\Omega_1}{\widetilde{\gamma}_2},\\
\mu_{\Delta 23} &= \frac{3}{2}\frac{\Omega_2}{\widetilde{\gamma}_2}\mu_{\Delta 33} + \Omega_1\frac{\Delta_2}{\gamma_2\widetilde{\gamma}_2}.
\end{aligned} \tag{40}$$

In the nonasymptotic limit where $\tau \sim \tau_m \sim \tau_p$, stationary solutions of $|\rho_{12}|$ and Δn have to be replaced by their transient expressions $|\rho_{12}(\tau,\tau_m)|$ and $\Delta n(\tau,\tau_m)$. When, $T \mapsto 0$, the line shape expression from Eq. (35) is formally equivalent to Eq. (8). A pulsed DR line shape is plotted in Fig. 10 (a) for small values of Rabi frequencies with a magnified

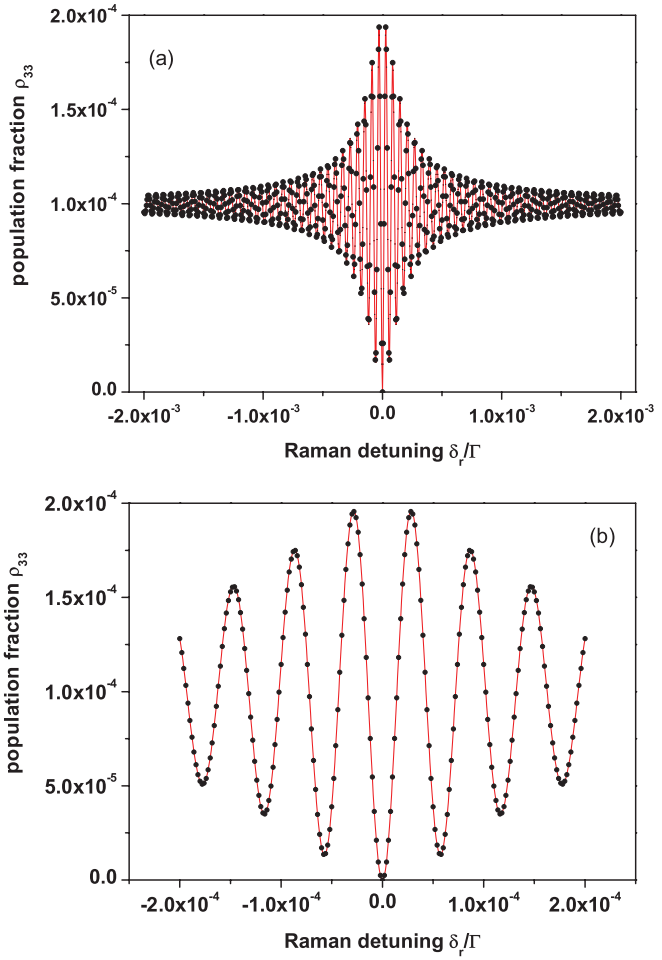

FIG. 10. (Color online) (a) Dark-resonance fringes in the weak field limit. (b) Frequency span of the line shape. Lines from Eq. (35) and dots (•) from Bloch's equations [Eq. (4)]. Common parameters: $\Gamma_{31} = \Gamma_{32} = \Gamma/2$, $\Delta_0 = 0$, $\gamma_c = 0$, and $T = 10\tau_p(0)$. In (a) and (b) Rabi frequencies $\Omega_1 = \Omega_2 = 0.005\Gamma$, free evolution time $T = 10\tau_p(0)$, and probe time $\tau_m \sim 0.004\tau_p(0)$. Very good agreement between Eqs. (4) and (35) results.

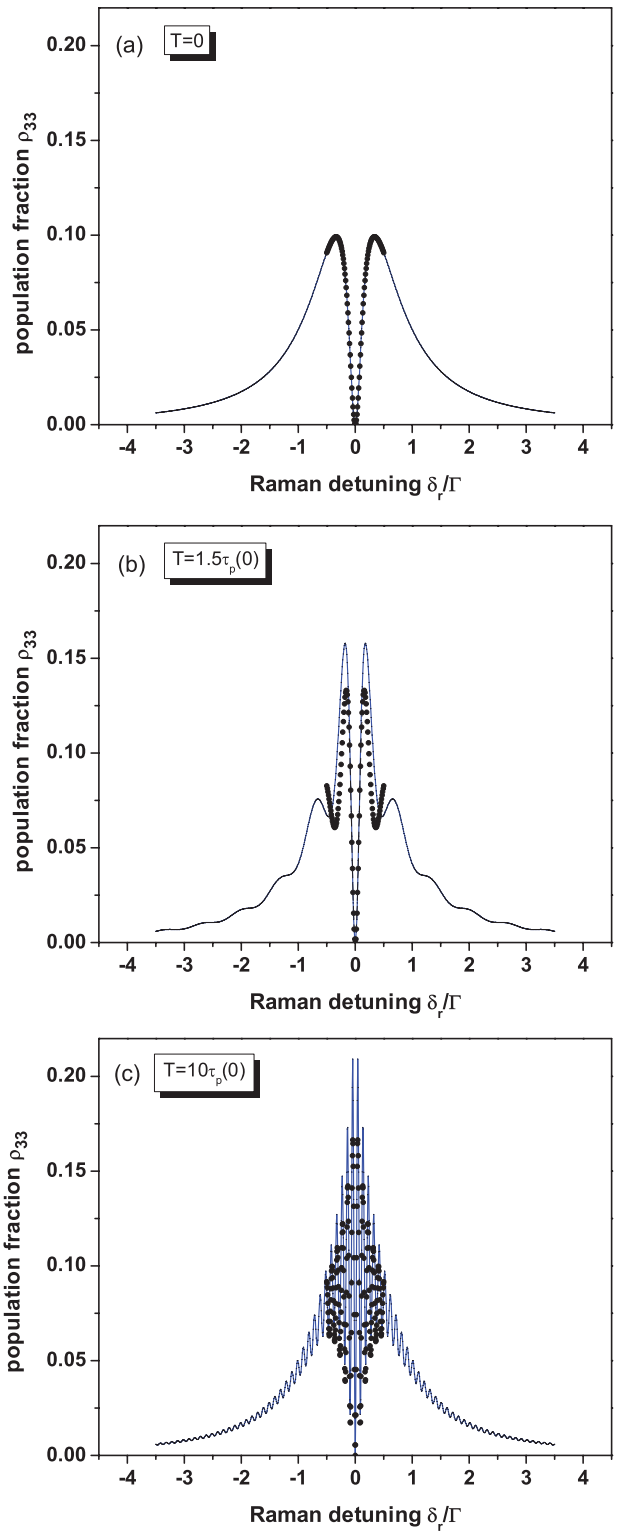

FIG. 11. (Color online) DR line shapes in strong laser fields computed from Eq. (35) vs Raman detuning for different values of Ramsey time T. Parameters $\Omega_1 = \Omega_2 = 0.2\Gamma$, $\Gamma_{31} = \Gamma_{32} = \Gamma/2$, $\Delta_0 = 0$, and $\gamma_c = 0$. Solid dots (•) from Bloch's equations [Eq. (4)] with $\tau = 10\tau_p(0)$. In (b) and (c) $\tau_m = 0.75\tau_p(0)$.

span on the central fringe in Fig. 10(b). In these plots, the agreement between Eq. (35) (solid red lines) and the Bloch's equations (dots •) is very accurate. We have also studied the role of the Ramsey time T on the DR line shape and amplitude. Figures 11(a)–11(c) show the signal amplitude versus the Raman detuning for different values of T. The fringe amplitude is always twice the amplitude in the cw regime when $2T > \Gamma_{\rm eff}^{-1}$ and $\gamma_c = 0$. A careful comparison between Fig. 10 and Figs. 11(b) and 11(c) show that for Rabi frequencies comparable to the Γ_{31}, Γ_{32} relaxation rates, i.e., when saturation becomes important, the limit $\tau_m \mapsto 0$ used to obtain Eq. (35) is no longer valid, and the effect of the readout duration pulse length τ_m has to be included into the analysis leading to a slight reduction of the fringe amplitude.

B. Stationary atomic or molecular Raman phase

The fringe signals appearing in the atomic observables are produced by the $\cos(\delta_r T - \Phi_{ij})$ terms appearing in the above expressions. Within a narrow region around the resonance, the line shape is entirely described by a phase given

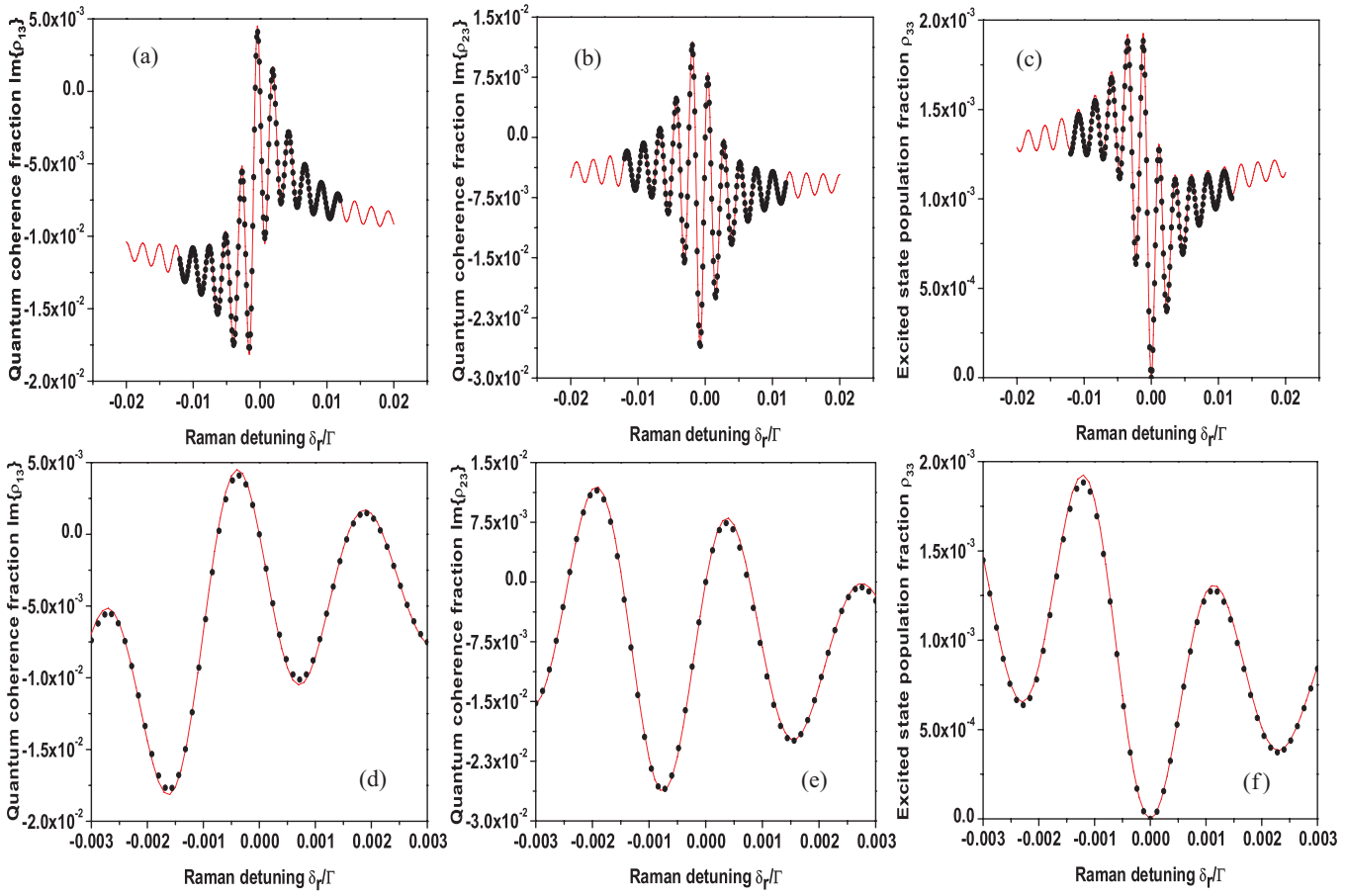

FIG. 12. (Color online) Asymmetric fringes observed on the imaginary parts of optical coherences, (a) $\mathrm{Im}\{\rho_{13}\}(T)$ and (b) $\mathrm{Im}\{\rho_{23}\}(T)$, and on the excited population (c) ρ_{33} vs Raman frequency detuning. In (d), (e), and (f), expanded views of the central resonance fringe for each observable are shown. Parameters $\Gamma_{31} = 0.8\Gamma$, $\Gamma_{32} = 0.2\Gamma$, $\Delta_0 = \Gamma$, $\gamma_c = 0$, $\Omega_1 = 5.10^{-2}\Gamma$, $\Omega_2 = 2.5 \times 10^{-2}\Gamma$, free evolution time $T = 10\tau_p(0)$, $\tau > 10\tau_p(\Gamma)$, and $\tau_m \sim 5.5 \times 10^{-3}\tau_p(\Gamma)$. Solid lines from the analytical forms of Eqs. (36), (37), and (35), respectively, are in good agreement with the solid dots (•) results from Bloch's equations [Eq. (4)].

by

$$\Phi_{33} = \mathrm{Arctan}\left[\frac{\mu_{\gamma 33}\mathrm{Im}\{\rho_{12}\} - \mu_{\Delta 33}\mathrm{Re}\{\rho_{12}\}}{\mu_{\gamma 33}\mathrm{Re}\{\rho_{12}\} + \mu_{\Delta 33}\mathrm{Im}\{\rho_{12}\}}\right],$$
$$\Phi_{13} = \mathrm{Arctan}\left[\frac{\mu_{\gamma 13}\mathrm{Im}\{\rho_{12}\} - \mu_{\Delta 13}\mathrm{Re}\{\rho_{12}\}}{\mu_{\gamma 13}\mathrm{Re}\{\rho_{12}\} + \mu_{\Delta 13}\mathrm{Im}\{\rho_{12}\}}\right], \quad (41)$$
$$\Phi_{23} = \mathrm{Arctan}\left[\frac{\mu_{\gamma 23}\mathrm{Im}\{\rho_{12}\} - \mu_{\Delta 23}\mathrm{Re}\{\rho_{12}\}}{\mu_{\gamma 23}\mathrm{Re}\{\rho_{12}\} + \mu_{\Delta 23}\mathrm{Im}\{\rho_{12}\}}\right].$$

In the adiabatic regime, for a first pulse producing a steady state and a second pulse with a short duration, the $|\rho_{12}|$ steady state solution of Eq. (27) leads to cw expressions of Φ_{ij} $(i,j = 1,2,3)$ where all time dependencies are absent. For clock engineering, it is important to quantify the shift of the central fringe when the common mode optical detuning $\Delta_1 \sim \Delta_2 \sim \Delta_0$ is scanned around the $\delta_r = 0$ resonant value. Within the limit of a long first pulse and a short second pulse, in the weak field regime and for a sufficiently large Ramsey time $[T \gg \tau_p(\Delta_0), \tau_m]$, the central fringe frequency-shift $\delta\omega_{ij}^{\mathrm{fr}}$ should be connected to the Φ_{ij} phase accumulation. Time-dependent Raman frequency shifts produced by short preparation pulses were examined in details in Refs. [57,58] using the Bloch vector model, but only for the excited state population. A complex wave-function formalism was also proposed for short pulses in [54] and extended in Ref. [55] to derive analytical time-dependent expressions of any frequency shift affecting the central fringe related to each possible observable.

Figures 12(a)–12(c) report the fringes appearing on the imaginary parts $\mathrm{Im}\{\rho_{13}\}(T)$, $\mathrm{Im}\{\rho_{23}\}(T)$ and on the excited state population $\rho_{33}(T)$ for an asymmetrical radiative configuration with $\Gamma_{31} = 0.8\Gamma$ and $\Gamma_{32} = 0.2\Gamma$, a detuned laser excitation $(\Delta_0 = \Gamma)$ with no Raman decoherence $(\gamma_c = 0)$. Plots from Figs. 12(d)–12(f) report a magnified span on the central fringe. The plots in Figs. 12(a) and 12(b) for the optical coherences show asymmetrical line shapes with the central fringe being blue or red shifted from the exact Raman resonance, a behavior different from that observed in the cw regime. For the excited state fraction plotted in Fig. 12(c) under the same conditions, the central fringe is not frequency shifted, as in the cw regime. These results point out, for the first time, that the imaginary parts of optical coherences, when individually probed, have a line shape different from that observed on the excited state response due to asymmetric decay rates by spontaneous emission.

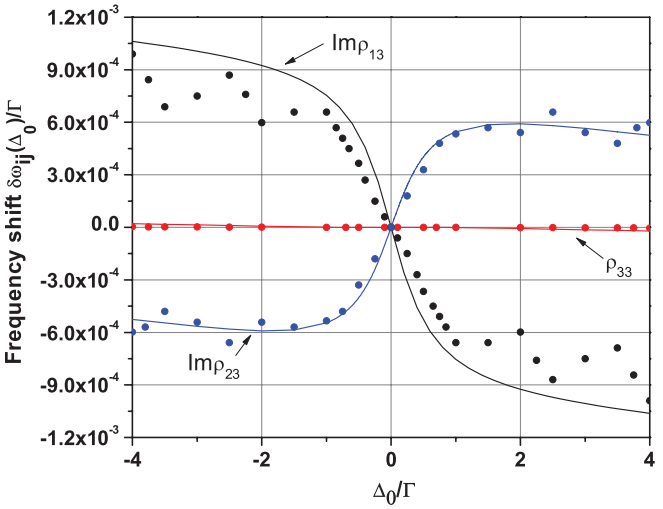

FIG. 13. (Color online) Exact numerical tracking of fringe frequency-shifts $\delta\omega_{13}^{\rm fr}$, $\delta\omega_{23}^{\rm fr}$, and $\delta\omega_{33}^{\rm fr}$ vs Δ_0 derived from Eqs. (35), (36), and (37) (solid lines). Parameters $\Gamma_{31} = 0.8\Gamma$, $\Gamma_{32} = 0.2\Gamma$, $\gamma_c = 5 \times 10^{-4}\Gamma$, $\Omega_1 = 5 \times 10^{-2}\Gamma$, $\Omega_2 = 3.7515 \times 10^{-2}\Gamma$, and $T = 10\tau_p(0)$. Solid dots (•) from Bloch's equations [Eq. (4)], where we use $\tau > 10\tau_p(\Gamma)$ and $\tau_m \sim 5.5 \times 10^{-3}\tau_p(\Gamma)$. The discrepancy between solid lines and dots are here due to the nonvanishing τ_m readout time required with a numerical integration of Bloch's equations.

This different behavior is also confirmed by the plots of Fig. 13 focusing on dark-resonance fringe frequency shifts versus the common mode optical detuning Δ_0 when assuming a small decoherence term $\gamma_c = 5 \times 10^{-4}\Gamma$. Figure 13 shows the numerical tracking of frequency shifts from the Eqs. (35), (36), and (37) analytical form compared to the integration of Bloch's equations [Eq. (4)] (solid dots) for a particular ratio between Rabi frequencies. Oscillations around the numerical track of frequency shifts are observed for large optical detunings due to the nonvanishing τ_m readout time used with Eqs. (4). Figure 14 evidences a very weak slope near

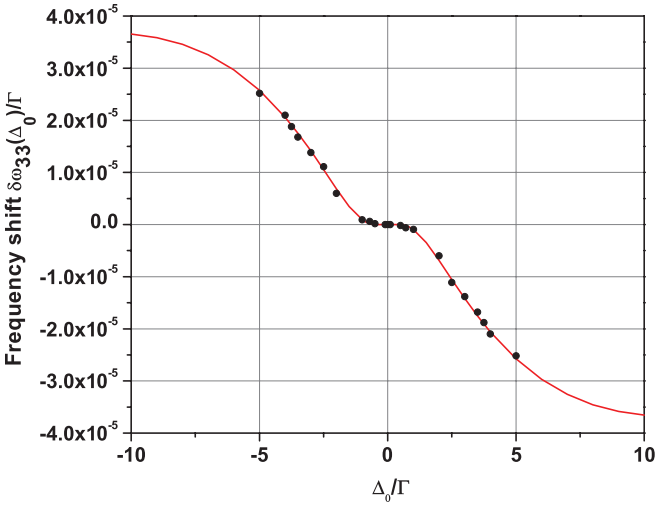

FIG. 14. (Color online) Exact numerical tracking of the dark-resonance fringe frequency-shift $\delta\omega_{33}^{\rm fr}$ vs Δ_0 derived from Eq. (35) (solid line). Solid dots (•) are plotted from Bloch's equations [Eq. (4)] with parameters as in Fig. 13.

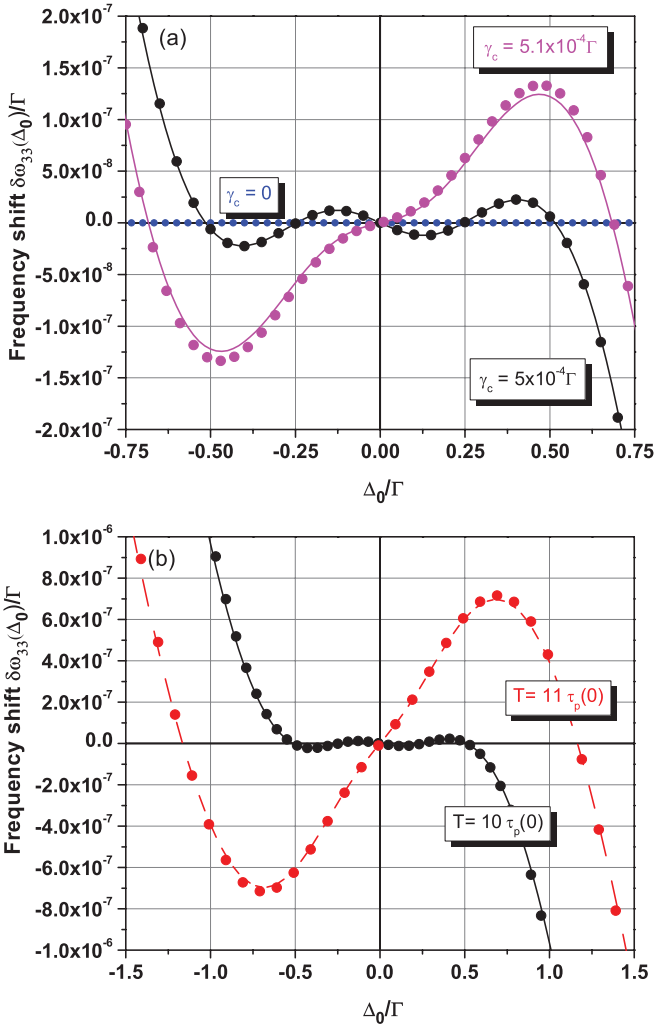

FIG. 15. (Color online) (a) Expanded view of the fringe frequency-shift numerical tracking $\delta\omega_{33}^{\rm fr}$ from Fig. 14 for various values of the small decoherence γ_c term. (b) Exact numerical frequency-shift $\delta\omega_{33}^{\rm fr}(\Delta_0)$ with different Ramsey time T for the particular ratio $\Omega_2/\Omega_1 \sim 0.75$ where $\Omega_1 = 5 \times 10^{-2}\Gamma$ and $\gamma_c = 5 \times 10^{-4}\Gamma$. Solid dots in the (a) and (b) cases are plotted from the analytical first order expansion of the Raman shift using Eq. (B10). Note the oscillating pattern with the small amplitude.

optical resonance; such dependence does not appear on the imaginary parts of the optical transmission. In absence of the γ_c decoherence, the excited state dependence was recently discussed in works [74,75] dealing with the time-dependant part of the Raman-Ramsey fringes reported earlier in [57,58].

A perturbative expansion of Eq. (35) in the Raman detuning parameter is required to derive the correct nonlinear behavior of the frequency shift versus the Δ_0 detuning, as reported in Eq. (B10). Those dependencies (solid dots) are plotted in Fig. 15 for $\Omega_2/\Omega_1 \sim 0.75$ and compared to the numerical tracking shift of the fringe minimum from Eq. (35) (solid lines). A nonlinear behavior with small oscillations around the optical resonance is correctly described. Increasing the time T, there is a small rotation of the frequency shift around the $\Delta_0 = 0$ common mode detuning as shown in Fig. 15(b). This dependence appears only for a nonvanishing γ_c decoherence

rate. For a given value of T, at specific values of the optical detuning, an exact cancellation of the frequency shift takes place as seen in Fig. 15(b).

VII. CONCLUSION

Three-level systems interacting with two coherent laser fields give rise to many phenomena, such as the Autler-Townes doublet, the dark or EIT resonance, and the Fano-Feshbach transition. In all of them the Raman coherence, playing an essential role, is highly sensitive to the parameters of the laser interaction and of the decoherence processes. The present work explored how those parameters may be tuned for future optical clock devices providing sensitive measurements of energy levels shifts in neutral atom clocks based on either fermionic or bosonic atomic species, for example, in dipolar traps [76] or in trapped ion clocks [77].

The three-level phenomena are well described by the formalism of the Bloch's equations in a semiclassical density matrix representation. From the exact resolution of Bloch's equations, we have derived general analytic expressions of the resonance line shapes observed in the steady state of different atomic observables. We have examined the linewidth and power broadening of the two-photon resonance. The precise dependence of the frequency shift associated to the Fano-Feshbach transition or to the EIT resonance, not appearing in a perturbation treatment, was discussed. We have examined the resonance fluorescence and frequency shift for a pulsed laser configuration in the adiabatic regime. The analytical but asymptotic solution allows us to write the line shape solution of the narrow quantum resonance leading to the formation of dark-resonance fringes. The pulsed sequence overcomes the power broadening mechanism of the continuous-wave excitation while allowing high contrasted signals in a saturation regime. In the weak field limit, signals in pulsed regimes are two times the continuous-wave signals, except for the decrease due to the Raman coherence relaxation within the atomic free evolution. The lower limit to the resonance linewidth is $1/2T$ to be compared to the Γ_{eff} limit in the steady-state case. The resonance shift is still proportional to the γ_c decoherence as for the steady state regime, but it is now diluted over the Ramsey time.

An important and original result of our analysis is that different atomic or molecular quantum observables (excited population, clock-state populations, and Raman coherence) experience different nonlinear line shapes and therefore different shifts of the clock resonance. Depending on the atomic parameters, the cw shifts of those observables may greatly differ in slopes, magnitude, or line shape. The shift amplitudes are also strongly related to the values of the decay channels, either balanced or unbalanced. For instance, while a large clock-population inversion is produced for unbalanced decay channels, a dispersive line shape is associated to its frequency shift. The detection of the Raman coherence exhibits a larger contrast, but it suffers usually from a systematic shift larger by an order of magnitude than that associated to the population detection. In the case of a very small decay rate for the Raman coherence, destructive interferences strongly reduce the cw frequency-shift sensitivity of the excited state compared to others observables. Thus the choice of the observable is very important for the proper operation of a three-level atomic or molecular clock. Additional technical constraints are associated to the requested detection tools of the chosen observable. For instance tracking the excited state population fraction by monitoring spontaneous emission or light transmission represents a sort of nondemolition quantum measurement avoiding the destructive readout associated to the lower-state clock projection.

The present solution can be extended to the case of a train of laser pulses having different frequencies, optical detunings, and phase steps as in Refs. [78,79], in order to design more elaborate combinations of optical transient nutations and free evolutions and to explore a more efficient detection scheme for very narrow transitions. For a treatment of the atom or molecule motion in matter wave interferometry [80], for instance, based on a pulsed EIT/Raman interaction with a resonant excitation scheme and using stimulated photon recoils to create a beam splitter, the Bloch's set of Eq. (4) requires both the introduction of the recoil shift into the laser detunings and the recoil spread among different atomic momentum classes produced by spontaneous emission yielding to a full set of quantum coupled equations [81].

ACKNOWLEDGMENTS

We would like to deeply thank Christof Janssen for a careful reading of the paper. T.Z.W is also extremely grateful to LPMAA for making possible the final completion of this work. T.Z.W would like to address his highest acknowledgment to J. Ye from JILA-NIST for supporting over a long time our ideas on three-level coherence for optical clocks.

APPENDIX A: GENERALIZED MULTIPHOTON STEADY-STATE RATE SOLUTIONS

The line shape expressions of Eqs. (8) and (21) may be recast in a different mathematical form using the generalized multiphoton rate solution of Ref. [43], later employed in Ref. [44] to establish conditions for the coherent population trapping in the steady-state regime. That analysis is based on three coupled equations for the $P_{ii}(Z)$, with $i = 1,2,3$, occupation probabilities of the three levels, equations written in the Laplace space of variable Z. This approach shown in Fig. (16) allows a reduction in the size of the linearly coupled equation system to be solved. The three-level populations are obtained as follows:

$$\rho_{ii} = \lim_{t\to\infty} P_{ii}(t) = \lim_{Z\to 0} Z P_{ii}(Z). \tag{A1}$$

From the steady-state solutions of Refs. [43,44], we obtain

$$\begin{aligned}
\rho_{33} &= \frac{w_{12}w_{23} + w_{13}(w_{12}+w_{23})}{3w_{13}w_{12} + \Gamma_{32}W_{11} + \Gamma_{31}W_{22} + 3w_{23}W_{33}},\\
\rho_{22} &= \frac{w_{12}w_{13} + \Gamma_{31}w_{12} + \Gamma_{32}(w_{13}+w_{12}) + w_{23}W_{33}}{3w_{13}w_{12} + \Gamma_{32}W_{11} + \Gamma_{31}W_{22} + 3w_{23}W_{33}},\\
\rho_{11} &= \frac{w_{12}w_{13} + \Gamma_{32}w_{12} + \Gamma_{31}(w_{23}+w_{12}) + w_{23}W_{33}}{3w_{13}w_{12} + \Gamma_{32}W_{11} + \Gamma_{31}W_{22} + 3w_{23}W_{33}},
\end{aligned} \tag{A2}$$

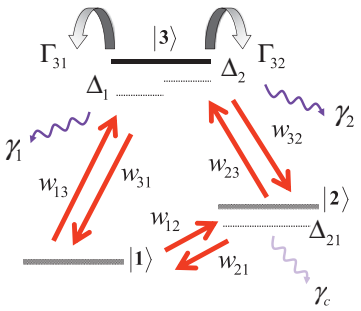

FIG. 16. (Color online) Definition of the w_{ij} transition rates within the three-level Λ configuration.

where the w_{ij} transition rates between each pair of states are defined in Fig. 16, and where

$$W_{11} = w_{13} + 2w_{12}, \quad W_{22} = w_{23} + 2w_{12}, \quad W_{33} = w_{13} + w_{12}. \tag{A3}$$

The expressions for the two-photon ($w_{12} \propto \Omega_1^2\Omega_2^2$) and one-photon ($w_{13} \propto \Omega_1^2, w_{23} \propto \Omega_2^2$) transitions rates are

$$w_{12} = 2\mathrm{Re}\left\{\frac{\Omega_1^2\Omega_2^2}{\xi_{31}\xi_{21}\xi_{32} + \Omega_1^2\xi_{31} + \Omega_2^2\xi_{32}}\right\},$$
$$w_{13} = 2\mathrm{Re}\left\{\frac{\Omega_1^2}{\xi_{31} + \frac{\Omega_2^2}{\xi_{21}+\frac{\Omega_1^2}{\xi_{32}}}}\right\} - w_{12}, \tag{A4}$$
$$w_{23} = 2\mathrm{Re}\left\{\frac{\Omega_2^2}{\xi_{32} + \frac{\Omega_1^2}{\xi_{21}+\frac{\Omega_2^2}{\xi_{31}}}}\right\} - w_{12}.$$

The detuning parameters ξ_{ij} are complex numbers depending on the system parameters

$$\xi_{31} = i\Delta_1 + \gamma_1, \quad \xi_{32} = -i\Delta_2 + \gamma_2, \quad \xi_{21} = i\Delta_{21} + \gamma_c = i(\Delta_1 - \Delta_2) + \gamma_c. \tag{A5}$$

The above expressions of the one- and two-photon rates point out the light-shift contributions to the eigenfrequencies of the three-level Λ system.

APPENDIX B: DARK-RESONANCE FRINGE FREQUENCY SHIFT

A. First order expression of $\delta\omega_{33}^{\mathrm{fr}}$

Equation (35) can be recast in the following form:

$$\rho_{33}(T) = \alpha_{33} + B_{33}\cos(U), \tag{B1}$$

where

$$B_{33} = \mu|\rho_{12}|e^{-\gamma_c T}, \quad \mu = \alpha_{33}\beta_{33}, \quad U = \delta_r T - \Phi_{33}. \tag{B2}$$

To establish the frequency shift, a track of the extremum of Eq. (35) produced by a differentiation versus δ_r leads to the following expression:

$$\rho_{33}^{'} = \alpha_{33}^{'} + \sqrt{B_{33}^{'2} + B_{33}^2 U'^2}\sin(U + \theta_{33}), \tag{B3}$$

with

$$\theta_{33} = -\arctan\left(\frac{B_{33}^{'}}{B_{33}U'}\right), \quad \text{if } T - \Phi_{33}^{'} < 0, \tag{B4}$$

$$\theta_{33} = -\arctan\left(\frac{B_{33}^{'}}{B_{33}U'}\right) + \pi, \quad \text{if } T - \Phi_{33}^{'} > 0. \tag{B5}$$

The $\rho_{33}^{'}$ derivative vanishes at

$$U + \theta_{33} + \eta_{33} = 0, \tag{B6}$$

where

$$\eta_{33} = \arcsin\left(\frac{\alpha_{33}^{'}}{\sqrt{B_{33}^{'2} + B_{33}^2 U'^2}}\right). \tag{B7}$$

Rewriting the cancellation condition as

$$\delta_r T - \Phi_{33} + \theta_{33} + \eta_{33} = 0, \tag{B8}$$

we apply a first order expansion of Eq. (B8) into the δ_r Raman detuning leading to the following $\delta\omega_{33}^{\mathrm{fr}}$ frequency shift:

$$\delta\omega_{33}^{\mathrm{fr}} \equiv \delta_r = \frac{\Phi_{33}(0) - \theta_{33}(0) - \eta_{33}(0)}{T - \Phi_{33}^{'}(0) + \theta_{33}^{'}(0) + \eta_{33}^{'}(0)}. \tag{B9}$$

If we neglect $\theta_{33}(0)$ and $\eta_{33}(0)$ terms, the discrepancy is, respectively, +6% and −13%. If we neglect the $\theta_{33}^{'}(0)$ or the $\eta_{33}^{'}(0)$ term, the error is below +0.4%. Thus at the 1% level of accuracy and at a common mode detuning that is small compared to spontaneous emission rates, we can rewrite the frequency-shift expression as

$$\delta\omega_{33}^{\mathrm{fr}} \approx \frac{\Phi_{33}(0) - \theta_{33}(0) - \eta_{33}(0)}{T - \Phi_{33}^{'}(0)}. \tag{B10}$$

B. Derivative terms

This subsection reports the functions appearing in Eq. (B10) and required to determine the frequency-shift $\delta\omega_{33}^{\mathrm{fr}}$ as a function of the common mode detuning Δ_0 and the system parameters. The additional functions may be obtained from the first order derivatives of the μ, Φ_{33}, $|\rho_{12}|$, and α_{33} functions calculated at $\delta_r = 0$. In order to simplify the mathematics, those functions are here reported for the case of a pure radiative process $\gamma_1 = \gamma_2, \tilde{\gamma}_1 = \tilde{\gamma}_2$, and supposing $\Delta_1 = \Delta_2 = \Delta_0$:

$$\Phi_{33}(0) = -\mathrm{Arctan}\left[\frac{\gamma_c\overline{\Delta}}{\gamma_{\mathrm{eff}}}\right], \tag{B11}$$

$$\mu^{'}(0) = \mu(0)\frac{\Delta_0\left(\tilde{\gamma}_1\Gamma + 3\Omega_1^2 - 3\Omega_2^2\right)}{\tilde{\gamma}_1\gamma_1\left(\tilde{\gamma}_1\Gamma + 3\Omega_1^2 + 3\Omega_2^2\right)}, \tag{B12}$$

$$\alpha'_{33}(0) = \frac{4\Delta_0\Omega_2^2\left[\Gamma\tilde{\gamma}_1 + \Delta n\left(\Gamma\tilde{\gamma}_1 + 6\Omega_1^2\right)\right]}{\Gamma\tilde{\gamma}_1\left[\Gamma\tilde{\gamma}_1 + 3\left(\Omega_1^2 + \Omega_2^2\right)\right]^2} + \frac{\tilde{\gamma}_1\left(\Omega_2^2 - \Omega_1^2\right)}{\left[\tilde{\gamma}_1{}^2\Gamma + 3\tilde{\gamma}_1\left(\Omega_1^2 + \Omega_2^2\right)\right]\Gamma_{\rm eff}^2}$$
$$\times\left\{\Delta_{11}S^{11} + \Delta_{22}S^{22} - \gamma_c\overline{\Delta}\overline{\gamma}_{22}S^{22} + \gamma_c\Delta_0\frac{2\overline{\Omega}_1^2}{\Gamma}(\overline{\gamma}_{11}S^{11} + \overline{\gamma}_{22}S^{22}) + \Delta n\left(\Delta_f - \frac{8\Delta_0\overline{\Omega}_1^2\left(\Gamma_{\rm eff}^2 - \gamma_c^2\right)}{4\Delta_0^2 + (1+2S)\Gamma^2}\right)\right.$$
$$+\frac{4\Delta_0 S\overline{\Omega}_1^2}{\left(1+2S+\frac{4\Delta_0^2}{\Gamma^2}\right)^2\Gamma^2}\left[\gamma_{22}^2\left(2+\frac{\tilde{\gamma}_1\Gamma_{32}}{\Omega_2^2}\right) - \gamma_{11}^2\left(2+\frac{\tilde{\gamma}_1\Gamma_{31}}{\Omega_1^2}\right)\right]$$
$$\left.-\frac{2\Delta_0\gamma_{22}^2\Gamma_{32}S^{\Lambda}}{\Gamma\Omega_2^2} + \frac{4\Delta_0\overline{\gamma}_{22}S^{22}\Gamma_{32}(2\Delta_0\overline{\Delta}\gamma_c + \Gamma\gamma_{\rm eff})}{\Gamma_{32}\left(4\Delta_0^2 + \Gamma^2\right) + 4\Gamma\Omega_2^2}\right\}, \tag{B13}$$

$$\Phi'_{33}(0) = -\frac{\overline{\Delta}^2\gamma_c\left(2\gamma_1^2\tilde{\gamma}_1 - 2\Delta_0^2\gamma_c + \gamma_1\tilde{\gamma}_1\gamma_c\right) + \gamma_{\rm eff}\left[2\gamma_1\tilde{\gamma}_1\left(\gamma_1 + \overline{\Omega}_1^2\gamma_c\right) - 2\Delta_0^2\gamma_{\rm eff} + \gamma_1\tilde{\gamma}_1\gamma_{\rm eff}\right]}{2\gamma_1^2\tilde{\gamma}_1\left(\overline{\Delta}^2\gamma_c^2 + \gamma_{\rm eff}^2\right)}, \tag{B14}$$

$$|\rho_{12}|'(0) = |\rho_{12}|(0)\left(\frac{\Delta_f}{\Gamma_{\rm eff}^2} - \frac{8\Delta_0\left\{4\Delta_0^2\gamma_c S + \Gamma\left[\gamma_{\rm eff}^2 + 3\gamma_c\gamma_{\rm eff}S - \gamma_c^2(1+2S)\right]\right\}\overline{\Omega}_1^2}{\left(1+2S+4\Delta_0^2/\Gamma^2\right)^2\Gamma^3\Gamma_{\rm eff}^2}\right.$$
$$\left.+\frac{\bar{\Delta}\left(\gamma_c - \gamma_{\rm eff} + 2\overline{\Omega}_1^2\gamma_c^2/\Gamma\right)}{\left(\bar{\Delta}^2\gamma_c^2 + \gamma_{\rm eff}^2\right)} + \frac{8\Delta_0\overline{\Omega}_1^2}{\Gamma^2\left(1+2S+4\Delta_0^2/\Gamma^2\right)}\right). \tag{B15}$$

These perturbative expressions were used to determine the $\delta\omega_{33}^{\rm fr}$ frequency shift plotted in Fig. 15 when $\Delta_0 \leqslant \Gamma$.

[1] J. B. M. Kellogg and S. Millman, Rev. Mod. Phys. **18**, 323 (1946).
[2] N. F. Ramsey, *Molecular Beams* (Oxford University Press, Oxford, 1956).
[3] A. D. Cronin, J. Schmiedmayer, and D. E. Pritchard, Rev. Mod. Phys. **81**, 1051 (2009).
[4] T. Hansch and P. Toschek, Z. Phys. **236**, 213 (1970).
[5] R. G. Brewer and E. L. Hahn, Phys. Rev. A **11**, 1641 (1975).
[6] R. M. Whitley and C. R. Stroud, Phys. Rev. A **14**, 1498 (1976).
[7] E. Arimondo and G. Orriols, Lett. Nuovo Cimento **17**, 333 (1976).
[8] G. Alzetta, A. Gozzini, L. Moi, and G. Orriols, Nuovo Cimento B **36**, 5 (1976).
[9] H. R. Gray, R. M. Whitley, and C. R. Stroud Jr., Opt. Lett. **3**, 218 (1978).
[10] G. Orriols, Nuovo Cimento B **53**, 1 (1979).
[11] V. Shah and J. Kitching, Adv. At. Mol. Phys. **59**, 21 (2010).
[12] I. Siemers, M. Schubert, R. Blatt, W. Neuhauser, and P. E. Toschek, Euro. Phys. Lett. **18**, 139 (1992).
[13] G. Janik, W. Nagourney, and H. Dehmelt, J. Opt. Soc. Am. B **2**, 1251 (1985).
[14] J. Vanier, Appl. Phys. B **81**, 421 (2005).
[15] P. Treutlein, P. Hommelhoff, T. Steinmetz, T. W. Hansch, and J. Reichel, Phys. Rev. Lett. **92**, 203005 (2004).
[16] D. M. Farkas, A. Zozulya, and D. Z. Anderson, Appl. Phys. B **101**, 701 (2010).
[17] R. Santra, E. Arimondo, T. Ido, C. H. Greene, and J. Ye, Phys. Rev. Lett. **94**, 173002 (2005).
[18] T. Hong, C. Cramer, W. Nagourney, and E. N. Forston, Phys. Rev. Lett. **94**, 050801 (2005).
[19] C. Champenois, G. Hagel, M. Houssin, M. Knoop, C. Zumsteg, and F. Vedel, Phys. Rev. Lett. **99**, 013001 (2007).
[20] E. Peik and C. Tamm, EuroPhys. Lett. **61**, 181 (2002).
[21] A. Greilich, R. Oulton, E. A. Zhukov, I. A. Yugova, D. R. Yakovlev, M. Bayer, A. Shabaev, A. L. Efros, I. A. Merkulov, V. Stavarache, D. Reuter, and A. Wieck, Phys. Rev. Lett. **96**, 227401 (2006).
[22] Z. Dutton, K. V. R. M. Murali, W. D. Oliver, and T. P. Orlando, Phys. Rev. B **73**, 104516 (2006).
[23] W. R. Kelly, Z. Dutton, J. Schlafer, B. Mookerji, T. A. Ohki, J. S. Kline, and D. P. Pappas, Phys. Rev. Lett. **104**, 163601 (2010).
[24] M. Santori, C. Tamarat, P. Neumann, J. Wrachtrup, D. Fattal, R. Beausoleil, J. Rabeau, P. Olivero, A. Greentree, S. Prawer, F. Jelezko, and P. Hemmer, Phys. Rev. Lett. **97**, 247401 (2006).
[25] X. Xu, B. Sun, P. R. Berman, D. G. Steel, A. S. Bracker, D. Gammon, and L. J. Sham, Nat. Phys. **4**, 692 (2008).
[26] M. Issler, E. M. Kessler, G. Giedke, S. Yelin, I. Cirac, M. D. Lukin, and A. Imamoglu, Phys. Rev. Lett. **105**, 267202 (2010).
[27] S. Weis, R. Rivire, S. Delglise, E. Gavartin, O. Arcizet, A. Schliesser, and T. J. Kippenberg, Science **330**, 1520 (2010).
[28] A. H. Safavi-Naeini, T. P. Mayer Alegre, J. Chan, M. Eichenfield, M. Winger, Q. Lin, J. T. Hill, D. E. Chang, and O. Painter, Nature (London) **472**, 69 (2011).
[29] R. Coussement, Y. Rostovtsev, J. Odeurs, G. Neyens, P. Mandel, G. Kozyreff, R. Shakhmuratov, and O. Kocharovskaya, Phys. Rev. Lett. **89**, 107601 (2002).
[30] T. J. Bürvenich, J. Evers, and C. H. Keitel, Phys. Rev. Lett. **96**, 142501 (2006).

[31] M. J. Mark, J. G. Danzl, E. Haller, M. Gustavsson, N. Bouloufa, O. Dulieu, H. Salami, T. Bergeman, H. Ritsch, R. Hart, and H. C. Nagerl, Appl. Phys. B **95**, 219 (2009).

[32] K. Winkler, G. Thalhammer, M. Theis, H. Ritsch, R. Grimm, and J. H. Denschlag, Phys. Rev. Lett. **95**, 063202 (2005).

[33] R. Dumke, J. D. Weinstein, M. Johanning, K. M. Jones, and P. D. Lett, Phys. Rev. A **72**, 041801(R) (2005).

[34] S. Moal, M. Portier, J. Kim, J. Dugue, U. D. Rapol, M. Leduc, and C. Cohen-Tannoudji, Phys. Rev. Lett. **96**, 023203 (2006).

[35] S. Moal, M. Portier, N. Zahzam, and M. Leduc, Phys. Rev. A **75**, 033415 (2007).

[36] B. Lounis and C. Cohen-Tannoudji, J. Phys. II **2**, 579 (1992).

[37] Y. Stalgies, I. Siemers, B. Appasamy, and P. E. Toschek, J. Opt. Soc. Am. B **15**, 2505 (1998).

[38] S. H. Autler and C. H. Townes, Phys. Rev. **100**, 703 (1955).

[39] U. Fano, Phys. Rev. **124**, 1866 (1961); H. Feshbach, Rev. Mod. Phys. **36**, 1076 (1964).

[40] E. Arimondo, Prog. Opt. **35**, 257 (1996).

[41] S. E. Harris, J. E. Field, and A. Imamoglu, Phys. Rev. Lett. **64**, 1107 (1990).

[42] M. Fleischhauer, A. Imamoglu, and J. P. Marangos, Rev. Mod. Phys. **72**, 633 (2005).

[43] S. Swain, J. Phys. B **13**, 2375 (1980).

[44] S. Swain, J. Phys. B **15**, 3405 (1982).

[45] P. L. Kelley, P. J. Harshman, O. Blum, and T. K. Gustafson, J. Opt. Soc. Am. B **11**, 2298 (1994).

[46] R. Wynands and A. Nagel, Appl. Phys. B **68**, 1 (1999).

[47] H. Lee, Y. Rostovtsev, C. J. Bednar, and A. Javan, Appl. Phys. B **76**, 33 (2003).

[48] M. J. McDonnell, D. N. Stacey, and A. M. Steane, Phys. Rev. A **70**, 053802 (2004).

[49] T. Zanon-Willette, Ph.D. thesis, LNE-SYRTE and UPMC, 2005, [http://tel.archives-ouvertes.fr/tel-00123499].

[50] T. Zanon, S. Guerandel, E. de Clercq, D. Holleville, N. Dimarcq, and A. Clairon, Phys. Rev. Lett. **94**, 193002 (2005).

[51] T. Zanon, S. Tremine, S. Guerandel, E. de Clercq, D. Holleville, N. Dimarcq, and A. Clairon, IEEE Trans. Instrum. Meas. **54**, 776 (2005).

[52] Xi Chen, G.-Q. Yang, J. Wang, and M.-S. Zhan, Chin. Phys. Lett. **27**, 113201 (2010).

[53] J. E. Thomas, P. R. Hemmer, S. Ezekiel, C. C. Leiby Jr., R. H. Picard, and C. R. Willis, Phys. Rev. Lett. **48**, 867 (1982).

[54] T. Zanon-Willette, A. D. Ludlow, S. Blatt, M. M. Boyd, E. Arimondo, and J. Ye, Phys. Rev. Lett. **97**, 233001 (2006).

[55] T. H. Yoon, Phys. Rev. A **76**, 013422 (2007).

[56] V. I. Yudin, A. V. Taichenachev, C. W. Oates, Z. W. Barber, N. D. Lemke, A. D. Ludlow, U. Sterr, Ch. Lisdat, and F. Riehle, Phys. Rev. A **82**, 011804 (2010).

[57] P. R. Hemmer, M. S. Shahriar, V. D. Natoli, and S. Ezekiel, J. Opt. Soc. Am. B **6**, 1519 (1989).

[58] S. M. Shahriar, P. R. Hemmer, D. P. Katz, A. Lee, and M. G. Prentiss, Phys. Rev. A **55**, 2272 (1997).

[59] C. Cohen-Tannoudji, J. Dupont-Roc, and G. Grynberg, *Atom-Photon Interactions* (Wiley, New York, 1998).

[60] E. T. Jaynes, Phys. Rev. **98**, 1099 (1955).

[61] H. C. Torrey, Phys. Rev. **76**, 1059 (1949).

[62] A. Abragam, *Principles of Nuclear Magnetism*, (Clarendon, Oxford, 1961); R. L. Schoemaker, in *Laser Coherence Spectroscopy*, edited by J. I. Steinfeld (Plenum, New York, 1978), p. 197.

[63] All quantities with an overbar are dimensionless.

[64] O. Kocharovskaya and P. Mandel, Phys. Rev. A **42**, 523 (1990).

[65] As mentioned in [37], in [5, 10] the Δ_{LS} Raman frequency shift was erroneously associated to the shift of the Raman peak.

[66] There is no internal shift of the EIT resonance when $\gamma_c = 0$ except if light shift produced by additional levels external to the Λ system is introduced into the Raman detuning [17, 54].

[67] E. De Clercq and P. Cerez, Opt. Com. **45**, 91 (1983).

[68] M. Fleischhauer and M. O. Scully, Phys. Rev. A **49**, 1973 (1994).

[69] A. G. Kofman, Phys. Rev. A **56**, 2280 (1997).

[70] H. R. Schlossberg and A. Javan, Phys. Rev. **150**, 267 (1966).

[71] H. R. Schlossberg and A. Javan, Phys. Rev. Lett. **17**, 1242 (1966).

[72] I. V. Jyotsna and G. S. Agarwal, Phys. Rev. A **52**, 3147 (1995).

[73] J. Vanier, A. Godone, and F. Levi, Phys. Rev. A **58**, 2345 (1998).

[74] J. Zhang and J. Chen, *Proceedings Frequency Control Symposium, 2007 Joint with the 21st European Frequency and Time Forum* (IEEE International, Geneva, 2007), p. 49.

[75] W. Wu and S. Peng, Chin. J. Electron. **19**, 229 (2010).

[76] A. Derevianko and H. Katori, Rev. Mod. Phys. **83**, 331 (2011).

[77] D. Leibfried, R. Blatt, C. Monroe, and D. Wineland, Rev. Mod. Phys. **75**, 281 (2003).

[78] B. J. Dalton, T. D. Kieu, and P. L. Knight, Opt. Acta. **33**, 459 (1986).

[79] L. M. K. Vandersypen and I. L. Chuang, Rev. Mod. Phys. **76**, 1037 (2005).

[80] C. J. Bordé, in *Atom Interferometry*, edited by P. Berman (Academic, San Diego, 1997), p. 257.

[81] A. Aspect, E. Arimondo, R. Kaiser, N. Vansteenkiste, and C. Cohen-Tannoudji, J. Opt. Soc. Am. B **6**, 2112 (1989).